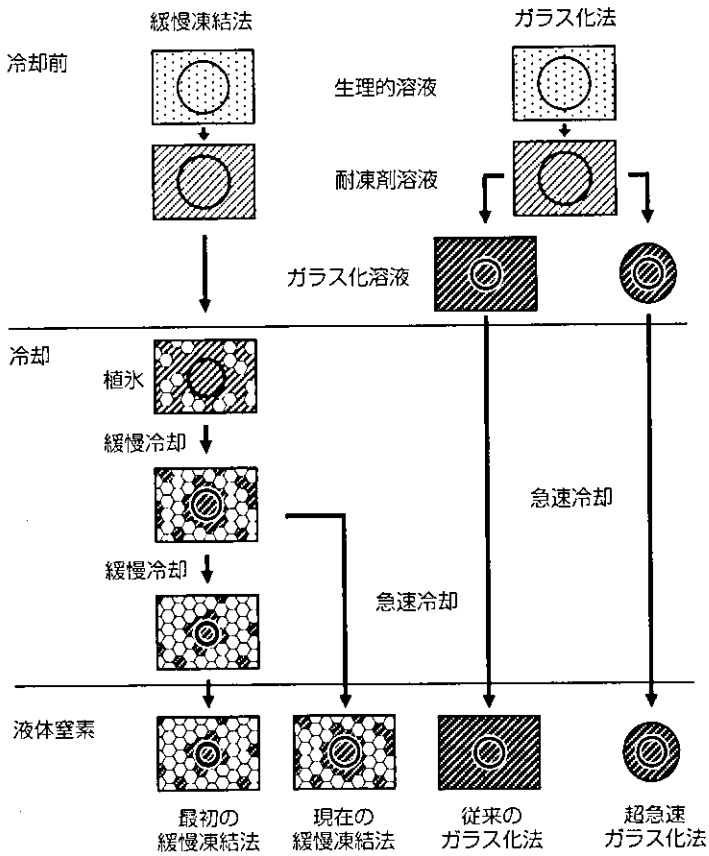

図２　種々の凍結保存法の模式図

る．しかし，1970 年代に胚の凍結保存が可能となったのちも，卵巣の凍結は困難であった．その後 1990 年代に入って研究の進展がみられ，とくにマウスにおいては，再現性の高い卵巣凍結法が開発されている[7]．しかし，用いられている卵巣は，幼若マウスのものである．

卵巣を凍結保存した場合にも，卵子や胚と同様のメカニズムによる傷害を考慮しなければならない．卵巣組織は卵子と比べると，けた違いに大きなサイズであり，組織全体に耐凍剤を透過させて脱水を促し，組織内の氷晶形成を防止するのは不可能である．実際には，細胞間隙に氷晶を形成させて細胞を脱水することによって細胞内氷晶を防止できると考えられている．したがって，凍結方法としては，緩慢凍結法が適していると思われる．組織内の氷晶は組織の内腔を広げて傷害を与える可能性があるが，卵巣では血管が再生されやすいので許容できるものと考えられている．卵子を卵巣組織ごと保存するためには，胞状卵胞内の GV 期卵子は耐凍剤を透過させ脱水を促すのが難しいため，表面近くにある小型の未熟な卵子がターゲットとなる．

卵巣をガラス化法で凍結しようとすると，耐凍剤の透過と脱水に時間を要し，高濃度の耐凍剤の毒性による傷害を受けやすいと思われていた．しかし，最近ガラス化法によって凍結したマウス卵巣からも，産子が得られている[8]．ヒトにおいても多くの検討がなされており，凍結保存した卵巣表面の組織片を自家移植することによって，卵胞発育が確認されているが，産子は得られていな

い．

おわりに

卵子凍結方法の有効性は，卵割，妊娠を経て，最終的には出産に至る割合によって確認しなければならない．しかし，現在のところ，その割合は低い値にとどまっている．卵子は，耐凍剤透過性が低いうえに，膨張に対する耐性も低いという，二重のハンディを持っている．そこで，比較的耐凍剤濃度の低い保存液でも細胞内氷晶を防止できる利点を持つ超急速ガラス化法に期待したい．現在までに，凍結卵子から生まれた子供について異常は報告されておらず，動物のデータを考慮しても，とくに卵子の凍結が多くの異常をもたらすとは思われない．しかし，ヒト卵子の症例は少なく，凍結保存の安全性の確認のためには，今後のデータの蓄積を待たなければならない．

文　献

1）Edashige K, et al : Cryobiology 38 : 273, 1999.
2）Pedro PB, et al : Cryobiology 35 : 150, 1997.
3）Pedro PB, et al : J Mamm Ova Res 14 : 66, 1997.
4）Kasai M : Reprod Med Biol 1 : 1, 2001.
5）宮野　隆，千本正一郎：産婦の世界 54 : 585, 2002.
6）Kim SS, et al : Fertil Steril 75 : 1049, 2001.
7）Sztein J, et al : Biol Reprod 58 : 1071, 1998.
8）Migishima F, et al : Biol Reprod 68 : 881, 2003.

Available online at www.sciencedirect.com
SCIENCE DIRECT®
Cryobiology 50 (2005) 93–102
CRYOBIOLOGY
www.elsevier.com/locate/ycryo

Water- and cryoprotectant-permeability of mature and immature oocytes in the medaka (*Oryzias latipes*)☆

Delgado M. Valdez Jr., Akira Miyamoto, Takao Hara, Shinsuke Seki, Magosaburo Kasai, Keisuke Edashige*

Laboratory of Animal Science, College of Agriculture, Kochi University, Nankoku, Kochi 783-8502, Japan

Received 20 September 2004; accepted 30 November 2004

Abstract

The permeability of the plasma membrane plays a crucial role in the successful cryopreservation of oocytes/embryos. To identify a stage feasible for the cryopreservation of teleost oocytes, we investigated the permeability to water and various cryoprotectants of medaka (*Oryzias latipes*) oocytes at the germinal vesicle (GV) and metaphase II (MII) stages. In sucrose solutions, the volume changes were greater in GV oocytes than MII oocytes. Estimated values for osmotically inactive volume were 0.41 for GV oocytes and 0.74 for MII oocytes. Water-permeability (μm/min/atm) at 25 °C was higher in GV oocytes (0.13 ± 0.01) than MII oocytes (0.06 ± 0.01). The permeability of MII oocytes to various cryoprotectants (glycerol, propylene glycol, ethylene glycol, and DMSO) was quite low because the oocytes remained shrunken during 2 h of exposure in the cryoprotectant solutions at 25 °C. When the chorion of MII oocytes was removed, the volume change was not affected, except in DMSO solution, where dechorionated oocytes shrunk and then regained their volume slowly; the P_{DMSO} value was estimated to be $0.14 \pm 0.01 \times 10^{-3}$ cm/min. On the other hand, the permeability of GV oocytes to cryoprotectants were markedly high, the P_s values ($\times 10^{-3}$ cm/min) for propylene glycol, ethylene glycol, and DMSO being 2.21 ± 0.29, 1.36 ± 0.18, and 1.19 ± 0.01, respectively. However, the permeability to glycerol was too low to be estimated, because GV oocytes remained shrunken after 2 h of exposure in glycerol solution. These results suggest that, during maturation, medaka oocytes become less permeable to water and to small neutral solutes, probably by acquiring resistance to hypotonic conditions before being spawned in fresh water. Since such changes would make it difficult to cryopreserve mature oocytes, immature oocytes would be more suitable for the cryopreservation of teleosts.

Keywords: Medaka; Oocyte; Cryoprotectant; Water; Permeability

Long-term storage of embryos is useful for the management of various stocks of model organisms. Such storage has been used for several mammalian embryos. However, the cryopreservation of

☆ Statement of funding: This work was supported by grants-in-aid for scientific research from the Ministry of Education, Culture, Sports, and Science of Japan, and Inamori Foundation.
* Corresponding author. Fax: +81 88 864 5219.
E-mail address: keisuke@cc.kochi-u.ac.jp (K. Edashige).

0011-2240/$ - see front matter © 2004 Elsevier Inc. All rights reserved.
doi:10.1016/j.cryobiol.2004.11.002

fish embryos has not succeeded because several factors are suspected to complicate the process [21]. Fish embryos have a large volume, a large amount of egg-yolk, and a thick chorion, form a complex structure during development, and are susceptible to chilling. Furthermore, fish embryos have several compartments with differing osmotic properties [7]. For instance, it is known in zebrafish embryos that, soon after the 50–70% epiboly stage, the yolk is surrounded by the multinucleated yolk syncytial layer, which is a permeability barrier to cryoprotectants [4,7]. For successful cryopreservation, the rapid movement of water and cryoprotectants through the membrane is essential.

The medaka (*Oryzias latipes*) is an important experimental fish for developmental biology, genetics, and physiology [2]. Strüssmann et al. [23] reported the successful cryopreservation of blastomeres of medaka embryos, but as with embryos of other teleosts, it is not possible to cryopreserve the whole embryo. Fortunately, however, medaka sperm can be easily cryopreserved [1]. Therefore, the long-term preservation of various stocks of medaka could be realized if the oocytes could be cryopreserved.

Unfortunately, fish oocytes have similar features to embryos that complicate cryopreservation, i.e., a large size and the presence of a yolk and chorion. However, oocytes are constituted from only a single compartment and do not have permeability barriers like the multinucleated yolk syncytial layer found in embryos. These features would be advantages for cryopreservation. The permeability of matured fish oocytes has been estimated in salmon [17,20], trout [9], and medaka [22]. In medaka, it has been shown that the cryoprotectant-permeability of the oocyte is lower than that of embryos [22]. Moreover, it is known that, in early stages of medaka embryos, the cryoprotectant-permeability of the plasma membrane increases as development proceeds [22]. Therefore, it seems that fish oocytes have the disadvantage of a lower cryoprotectant-permeability. However, the oocytes used in the studies mentioned above were ovulated, and were in the stage where they were just about to be exposed to non-isotonic conditions, that is, fresh water (hypotonic). Therefore, it would be reasonable to assume that such matured oocytes have already acquired the ability to tolerate non-isotonic conditions. On the other hand, fish oocytes at earlier stages might not have acquired this tolerance and might have different permeability properties from matured ones. However, no information is available on the permeability of immature oocytes in fish.

In this study, we examined the water- and cryoprotectant-permeability of medaka oocytes at the germinal vesicle (GV) stage and the metaphase II (MII) stage in order to identify a stage feasible for oocyte cryopreservation.

Materials and methods

Collection of oocytes

About 20–100 matured orange-red type medaka, purchased from a local fish dealer, were maintained in 60-liter aquariums under 14-h light and 10-h dark periods at 25 °C. Newly ovulated MII oocytes were obtained from ovarian cavities of actively spawning females humanely killed 1 h before the start of the light period and kept in saline formulated for medaka oocytes (SMO medium) [13] at room temperature prior to use. The composition of the solution is as follows; NaCl, 6.50 g; KCl, 0.40 g; $CaCl_2 \cdot 2H_2O$, 0.15 g; $MgSO_4 \cdot 7H_2O$, 0.15 g; $NaHCO_3$, 1.00 g; phenol red, 0.015 g; in 1 L of distilled water with 5 mM Hepes–HCl, pH 7.0 [13]. The oocytes were used for experiments within 2 h of collection. Fully grown GV oocytes were obtained from ovaries of actively spawning females humanely killed 1–3 h before the start of the dark period, and cultured in 90% tissue culture medium (TCM)-199 with Earle's salts (Cat. No. 31100-035, Gibco Invitrogen, Carlsbad, CA, USA) [12] at 25 °C for 2–4 h prior to use.

In some experiments, the chorion of MII oocytes was removed using microsurgical scissors (6 mm) and tweezers (0.1 × 0.06 mm tip, 11 cm length) [13]. After being kept in SMO medium at room temperature for 30 min, dechorionated oocytes were examined and the non-activated ones (with small oil droplets dispersed in the cytoplasm)

selected and used for experiments within 1.5 h. We did not measure volume changes of dechorionated GV oocytes in sucrose or cryoprotectant solutions because we could not surgically or enzymatically remove the chorion of GV oocytes without causing damages.

Osmotically inactive fractions

Intact MII oocytes were placed in SMO medium containing 0.26 and 1.26 Osm/kg sucrose (0.24 and 0.91 M, respectively), excluding the 0.24 Osm/kg contributed by the SMO medium, or in SMO medium diluted with distilled water (×0.50 or ×0.63, 0.12 or 0.15 Osm/kg, respectively) at 25 ± 1 °C until the oocytes were equilibrated with the solutions (for 3 h). GV oocytes were placed in 90% (v/v) TCM-199 containing 0.23 and 1.23 Osm/kg sucrose (0.21 and 0.89 M, respectively), excluding the 0.27 Osm/kg contributed by the 90% TCM-199 medium, or in 90% TCM-199 diluted with distilled water (×0.44 or ×0.56, 0.12 or 0.15 Osm/kg, respectively), at 25 °C for 2 h. The osmolality of sucrose was calculated from published data on the colligative properties of sucrose in aqueous solutions [27]. The osmolality of the basic media and diluted basic media was measured with an osmometer (OM801; Vogel, Giessen, Germany). Total osmolality of the solutions is shown in Table 1. We assumed that the osmolality of oocyte cytoplasm was equilibrated with that of basic media (GV oocytes, 0.27 Osm/kg; MII oocytes, 0.24 Osm/kg) because, until use for experiments, GV oocytes were incubated in 90% TCM-199 medium for 2–3 h and MII oocytes were incubated in SMO medium for 1–2 h; those periods were sufficient for the oocytes to be equilibrated with the basic media. The microscopic images of the oocytes were recorded using a time-lapse video recorder (ETV-820, Sony, Tokyo, Japan) for 2–3 h during exposure. The cross-sectional area of the oocyte was measured using an image analyzer (VM-50, Olympus, Tokyo, Japan). Relative cross-sectional area, S, is expressed by

Table 1
The osmolality of solutions used

Diluent			Solute		Total osmolality (Osm/kg)
Basic medium	Tonicity	Osmolality[a] (Osm/kg)	Name	Osmolality (Osm/kg)	
SMO	×0.50	0.12	—	—	0.12
	×0.63	0.15	—	—	0.15
	×1.00	0.24	—	—	0.24
	×1.00	0.24	0.24 M sucrose	0.26[b]	0.50
	×1.00	0.24	0.91 M sucrose	1.26[b]	1.50
	×1.00	0.24	8% ethylene glycol	1.61[b]	1.85
	×1.00	0.24	10% glycerol	1.59[b]	1.83
	×1.00	0.24	10% propylene glycol	1.56[b]	1.80
	×1.00	0.24	9.5% DMSO	1.55[c]	1.79
90% TCM-199	×0.44	0.12	—	—	0.12
	×0.56	0.15	—	—	0.15
	×1.00	0.27	—	—	0.27
	×1.00	0.27	0.21 M sucrose	0.23[b]	0.50
	×1.00	0.27	0.89 M sucrose	1.23[b]	1.50
	×1.00	0.27	8% ethylene glycol	1.61[b]	1.88
	×1.00	0.27	10% glycerol	1.59[b]	1.86
	×1.00	0.27	10% propylene glycol	1.56[b]	1.83
	×1.00	0.27	9.5% DMSO	1.55[c]	1.82

[a] Osmolality measured with a freezing point depression osmometer.
[b] Osmolality calculated from published data on the colligative properties of the solutes in aqueous solutions [27].
[c] Osmolality measured with a vapor pressure osmometer.

dividing it by the initial area of the same oocyte. The relative volume was obtained from $V = S^{3/2}$. Osmotically inactive fractions (v_b) were obtained from Boyle–van't Hoff plots.

Water- and cryoprotectant-permeability of oocytes

Oocytes placed in isotonic basic medium (SMO medium or 90% TCM-199 medium) were introduced into basic media containing sucrose or cryoprotectants (200 μl) covered with mineral oil in a Petri dish (35 × 10 mm) at 25 ± 1 °C for 1 h (GV oocytes) or 2 h (MII oocytes), with a minimal amount of isotonic solution using a pipette. The microscopic images of the oocytes were recorded using a time-lapse video recorder for 1 or 2 h during exposure. The cross-sectional area of the oocyte was measured and the relative volume at various time points of exposure was obtained as described above. Hydraulic conductivity (L_P) and cryoprotectant-permeability (P_s) were determined by fitting water and solute movements using a two-parameter formalism as described elsewhere [3]. In principle, the use of the Kedem–Katchalsky formalism [14], which incorporates a solvent–solute interaction parameter (sigma) for calculating water- and cryoprotectant-permeability, would be appropriate. However, determination of a reliable sigma value is quite difficult [15]. Since we require only a phenomenological description of the oocyte behavior, we used the two-parameter formalism for the calculation of water- and cryoprotectant-permeability. L_P values of intact and dechorionated MII oocytes were calculated from volumetric changes in SMO medium containing 1.26 Osm/kg sucrose, excluding the 0.24 Osm/kg contributed by the SMO medium, and that of GV oocytes was calculated from volumetric changes in 90% TCM-199 medium containing 1.23 Osm/kg sucrose, excluding the 0.27 Osm/kg contributed by the 90% TCM-199 medium. The P_s for each cryoprotectant was calculated from volumetric changes in a medium containing 10% (v/v) glycerol, 10% (v/v) propylene glycol, 8% (v/v) ethylene glycol, or 9.5% (v/v) DMSO. The volume percentage was varied to prepare cryoprotectant solutions with similar osmolality (Table 1). The osmolality contributed by glycerol, propylene glycol, ethylene glycol, and DMSO was 1.59, 1.56, 1.61, and 1.55 Osm/kg, respectively, excluding the osmolality contributed by the media (Table 1). Total osmolality of the solutions is shown in Table 1. The osmolality of glycerol, propylene glycol, and ethylene glycol was calculated from published data on the colligative properties of each cryoprotectant in aqueous solutions [27]. The osmolality of 9.5% DMSO in an aqueous solution was measured with a vapor pressure osmometer (Vapro 5520; Wescor, Logan, UT, USA). Other various constants and parameters are listed in Table 2.

Results

Osmotically inactive fractions of oocytes at the GV and MII stages

Fig. 1 shows the Boyle–van't Hoff plots of oocytes at the GV and MII stages. Oocytes at both stages shrunk in hypertonic solutions and swelled

Table 2
Constants and parameters used for fitting permeability parameters

Symbol	Meaning	Values
R	Gas constant (liter atm K^{-1} mol^{-1})	8.206×10^{-2}
T	Absolute temperature	298 K
$\overline{V}_w$	Partial molar volume of water	0.018 L/mol
$\overline{V}_{EG}$	Partial molar volume of ethylene glycol[a]	0.054 L/mol
$\overline{V}_{GLY}$	Partial molar volume of glycerol[a]	0.071 L/mol
$\overline{V}_{PG}$	Partial molar volume of propylene glycol[a]	0.070 L/mol
$\overline{V}_{DMSO}$	Partial molar volume of DMSO[b]	0.069 L/mol

[a] Partial molar volumes of cryoprotectants from Wolf et al. [27].
[b] Partial molar volume of DMSO from Mazur [19].

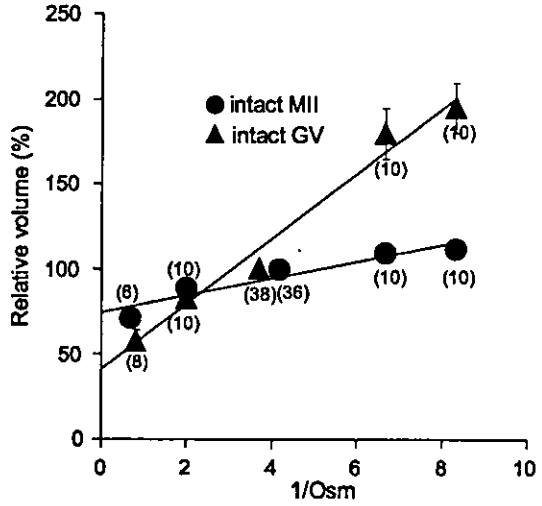

Fig. 1. Boyle-van't Hoff plots of the relative volume of intact medaka oocytes at the germinal vesicle (closed triangles) and metaphase II stages (closed circles). Oocytes at the germinal vesicle stage were equilibrated in 90% TCM-199 medium containing different concentrations of sucrose or in 90% TCM-199 diluted with distilled water at 25 °C for 2 h. Intact oocytes at the metaphase II stage were equilibrated in SMO medium containing different concentrations of sucrose or in SMO medium diluted with distilled water at 25 °C for 3 h. Data are indicated as means of relative volumes ± SD. Numbers in parentheses indicate the number of oocytes used.

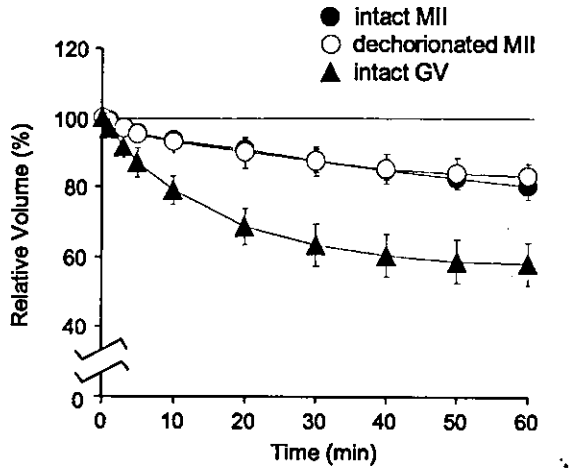

Fig. 2. Change in cell volume of intact (closed circles) and dechorionated (open circles) medaka oocytes at the metaphase II stage and intact oocytes at the germinal vesicle stage (closed triangles) in a hypertonic sucrose solution. Intact and dechorionated MII oocytes incubated in SMO medium (0.24 Osm/kg) at 25 °C were exposed to SMO medium containing 1.26 Osm/kg sucrose at 25 °C for 1 h. Intact GV oocytes cultured in 90% TCM-199 medium (0.27 Osm/kg) were exposed to 90% TCM-199 medium containing 1.23 Osm/kg sucrose at 25 °C for 1 h. Data are indicated as means of relative volumes ± SD. Data of intact MII oocytes and GV oocytes were from 10 oocytes and those of dechorionated MII oocytes were from six oocytes.

in hypotonic solutions. However, changes in equilibrated volume of MII oocytes in solutions of various osmolalities were much smaller than those of GV oocytes, suggesting that the v_b value of GV oocytes is smaller than that of MII oocytes. Actually, the calculated value for v_b of GV oocytes was 0.41 and the value of r^2 of the regression line was 0.98, whereas that of MII oocytes was 0.74 and the value of r^2 of the regression line was 0.90.

We used these v_b values for calculation of the water- and cryoprotectant-permeability of the oocytes.

Permeability to water of oocytes at the GV and MII stages

Fig. 2 shows changes in the volume of oocytes at the GV and MII stages in media containing sucrose (the osmolality of both solutions was 1.50 Osm/kg). MII oocytes shrunk slowly and the change in volume did not differ between intact and dechorionated oocytes. This suggests that the chorion does not affect the water-permeability of MII oocytes. On the other hand, GV oocytes shrunk more rapidly, perhaps due to differences in the osmotically inactive volume and water-permeability. As described above, the value for v_b of MII oocytes was much higher than that of GV oocytes (Fig. 1). L_P values of intact and dechorionated MII oocytes were the same (0.06 ± 0.01 μm/min/atm). This value was much lower than the value for GV oocytes (0.13 ± 0.01 μm/min/atm) (Table 3). These results show that water permeates GV oocytes much faster than MII oocytes.

Permeability to cryoprotectants of oocytes at the MII stage

Fig. 3 shows volume changes of intact and dechorionated oocytes at the MII stage in SMO medium containing glycerol, propylene glycol, ethylene glycol, or DMSO at 25 °C. In glycerol

Table 3
Water-permeability of medaka oocytes

Oocytes	L_P (μm/min/atm)
Intact MII oocytes	0.06 ± 0.01
Dechor MII oocytes[a]	0.06 ± 0.01
GV oocytes	0.13 ± 0.01*

[a] Dechorionated MII oocytes.
* Significantly different from intact and dechorionated MII oocytes (Student's t test, $P < 0.01$).

solution, both types of oocytes shrunk slowly and did not regain their volume during 2-h exposure, suggesting that glycerol permeates both oocytes quite slowly (Fig. 3A). Since we did not observe a reswelling phase on permeation of the glycerol during 2-h exposure, we could not calculate glycerol-permeability for the two types of oocytes. MII oocytes in propylene glycol and ethylene glycol solutions also shrunk slowly and did not regain their volume regardless of the presence or absence of the chorion (Figs. 3B and C), suggesting that propylene glycol and ethylene glycol also permeate MII oocytes quite slowly. Thus, we could not calculate the cryoprotectant-permeability of MII oocytes from these data. In DMSO solution, intact oocytes also remained shrunken during 2-h exposure whereas dechorionated oocytes shrunk but regained their volume thereafter (Fig. 3D), suggesting that DMSO permeated dechorionated oocytes. The value for P_{DMSO} of the dechorionated oocytes was calculated to be $0.14 \pm 0.01 \times 10^{-3}$ cm/min (Table 4).

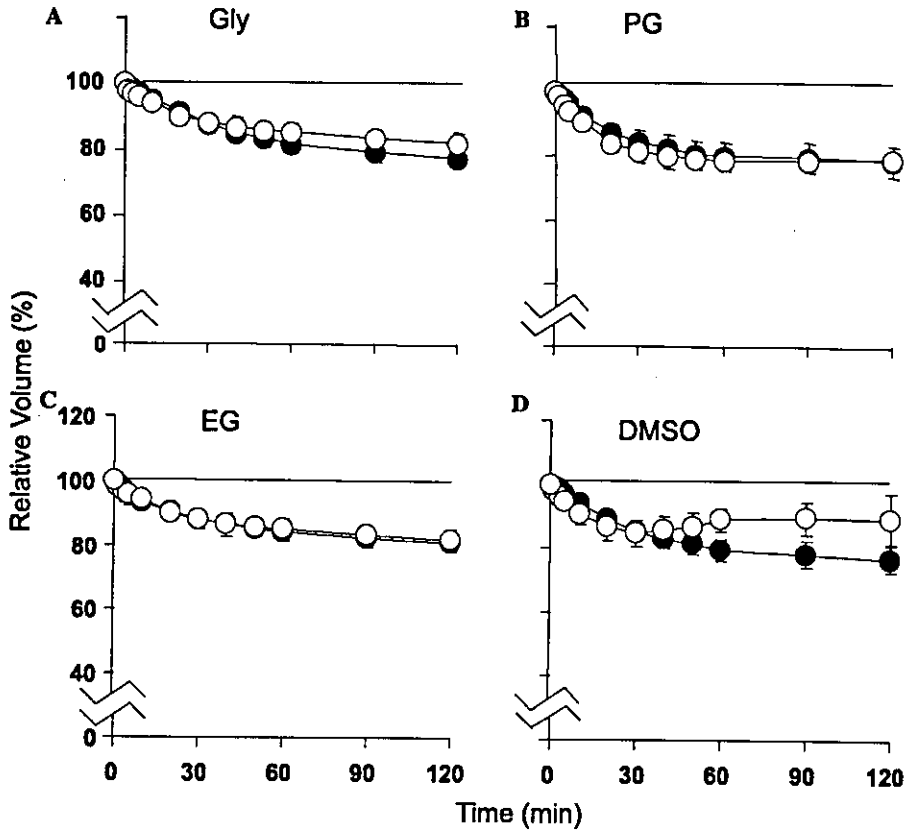

Fig. 3. Change in cell volume of intact (closed circles) and dechorionated (open circles) medaka oocytes at the metaphase II stage in 10% glycerol (A), 10% propylene glycol (B), 8% ethylene glycol (C), and 9.5% DMSO (D) solutions. Oocytes were exposed to SMO medium containing various cryoprotectants at 25 °C for 2 h. Data are indicated as means of relative volumes ± SD. Data of intact MII oocytes were from 10 oocytes and those of dechorionated MII oocytes were from six oocytes.

Table 4
Permeability ($\times 10^{-3}$ cm/min) of medaka oocytes to cryoprotectants

Oocytes	P_{GLY}[a]	P_{PG}[b]	P_{EG}[c]	P_{DMSO}[d]
Intact MII oocytes	nd[e]	nd	nd	nd
Dechor MII oocytes[f]	nd	nd	nd	0.14 ± 0.01
GV oocytes	nd	2.21 ± 0.29*	1.36 ± 0.18*	1.19 ± 0.01*

[a] Glycerol-permeability.
[b] Propylene glycol-permeability.
[c] Ethylene glycol-permeability.
[d] DMSO-permeability.
[e] Not determined.
[f] Dechorionated MII oocytes.
* Significantly different from intact and dechorionated MII oocytes (Student's t test, $P < 0.01$).

These results suggest that the polyol-permeability of MII oocytes is very low whereas the DMSO-permeability is relatively high but that the chorion hinders the permeation of DMSO.

Permeability to cryoprotectants of oocytes at the GV stage

Fig. 4 shows volume changes of GV oocytes in 90% TCM-199 containing glycerol, propylene glycol, ethylene glycol, or DMSO at 25 °C. In glycerol solution, GV oocytes shrunk slowly and did not regain their volume during 2-h exposure (Fig. 4A) similar to MII oocytes, suggesting that glycerol permeates GV oocytes quite slowly. On the other hand, in propylene glycol (Fig. 4B), ethylene glycol (Fig. 4C), and DMSO (Fig. 4D) solutions, GV oocytes shrunk and regained their volume, suggesting that these cryoprotectants permeate GV oocytes much faster than MII oocytes. Values for propylene glycol-, ethylene glycol-, and DMSO-permeability of GV oocytes were 2.21 ± 0.29, 1.36 ± 0.18, and $1.19 \pm 0.01 \times 10^{-3}$ cm/min, respectively (Table 4).

These results show that GV oocytes are permeable to various cryoprotectants.

Discussion

As an essential step for obtaining L_P and P_S for medaka oocytes, we first measured v_b for GV oocytes and MII oocytes. From the data shown in Fig. 1, the v_b value of GV oocytes was estimated to be 0.41. This value would be reliable, because the volumes of GV oocytes equilibrated in both hypertonic and hypotonic solutions were linearly arranged in the Boyle-van't Hoff plots ($r^2 = 0.98$). On the other hand, the v_b value for MII oocytes was estimated to be 0.74, which was remarkably higher than the value for GV oocytes (0.41). This value for MII oocytes was larger than that of matured zebrafish oocytes (0.64) [28]. Since it is unlikely that the amount of materials in medaka oocytes actually increases that much during a short period (10 h) of final maturation, it may show the physiological changes of medaka oocytes just before spawning. Moreover, in the Boyle-van't Hoff plots (Fig. 1), equilibrated volumes of MII oocytes in hypotonic solutions were smaller than those expected from equilibrated volumes in hypertonic solutions. This suggests that, during the final maturation stage, medaka oocytes acquire the ability to resist osmotic changes, especially in hypotonic conditions. This seems reasonable because medaka oocytes are exposed to fresh water at spawning, and thus oocytes would be ruptured if they could not acquire such tolerance. If so, such a change in the membrane permeability in maturing oocytes is expected to occur in other fresh water fish also. In zebrafish, it has been shown that embryos do not swell in hypotonic solutions whereas they shrink in hypertonic solutions [8]. However, the mechanism by which oocytes and embryos resist osmotic swelling in fresh water remains to be elucidated. In any case, the observations and speculation made here strongly suggest that the v_b value of medaka MII oocytes was actually overestimated. In this case, the water- and cryoprotectant-permeability of the MII oocytes would be

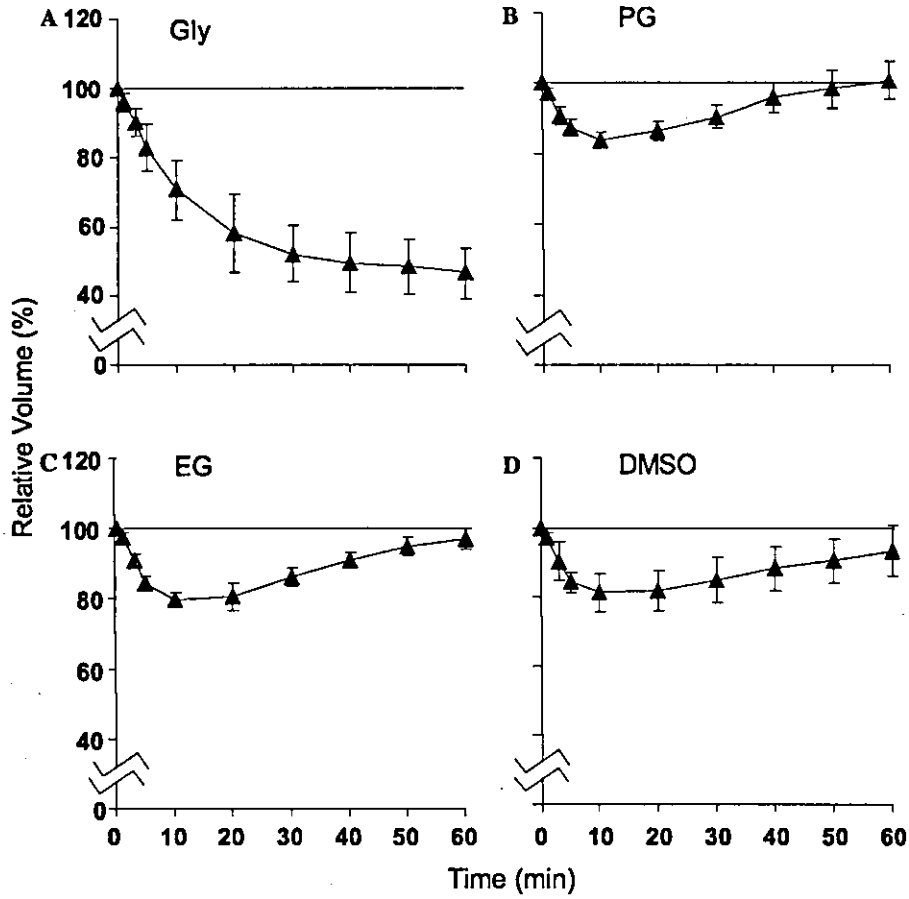

Fig. 4. Change in cell volume of intact medaka oocytes at the germinal vesicle stage in 10% glycerol (A), 10% propylene glycol (B), 8% ethylene glycol (C), and 9.5% DMSO (D) solutions. Oocytes were exposed to 90% TCM-199 medium containing various cryoprotectants at 25 °C for 1 h. Data are indicated as means of relative volumes ± SD. Data of GV oocytes in glycerol, propylene glycol, and DMSO solutions were from 10 oocytes, and those in ethylene glycol solutions were from nine oocytes.

slightly overestimated. However, the permeability values obtained for medaka MII oocytes were low.

The L_P of medaka MII oocytes obtained in this study was 0.06 ± 0.01 μm/min/atm, and the removal of the chorion from the oocytes did not affect the water-permeability (Fig. 2, Table 3). This shows that the chorion does not hinder water movement. Harvey and Chamberlain [10] also reported that the chorion of zebrafish embryos was freely permeable to water. The L_P value obtained (0.06 ± 0.01 μm/min/atm) is comparable to that for pacific salmon oocytes (0.08 μm/min/atm; a value converted using an equation reported by Leibo [16]; 1 μm/min/atm = 22.4 μm/s) [20] or zebrafish embryos from the 75% epiboly to three-somite stage (0.05 ± 0.01 μm/min/atm) [6]. On the other hand, the L_P of medaka GV oocytes obtained in this study (0.13 ± 0.01 μm/min/atm) (Fig. 2 and Table 3) was more than twice that of MII oocytes. This higher water-permeability of medaka GV oocytes would be an advantage over MII oocytes for cryopreservation.

The cryoprotectant-permeability of MII oocytes was quite low. Except for the DMSO-permeability of dechorionated MII oocytes, we could not calculate P_s values because oocytes did not regain their volumes during 2-h exposure in cryoprotectant solutions. The shrinkage curves of intact

and dechorionated MII oocytes in glycerol, propylene, glycol, and ethylene glycol solutions were substantially the same. As an exception, dechorionated MII oocytes in DMSO solution shrunk and regained their volume although intact MII oocytes remained shrunken. This shows that DMSO permeates MII oocytes but the chorion hinders the permeation. Similar results have already been reported for zebrafish embryos [11]. However, the DMSO-permeability of dechorionated medaka MII oocytes was not high ($0.14 \pm 0.01 \times 10^{-3}$ cm/min) (Table 4). Thus, it will be difficult to introduce an amount of cryoprotectant into medaka MII oocytes sufficient for cryopreservation regardless of the absence of their chorion.

Compared with MII oocytes, GV oocytes, with the chorion, had a much higher cryoprotectant-permeability; the P_s values ($\times 10^{-3}$ cm/min) for propylene glycol, ethylene glycol, and DMSO being 2.21 ± 0.29, 1.36 ± 0.18, and 1.19 ± 0.01, respectively (Fig. 4, Table 4). It has been reported that the DMSO-permeability of medaka oocytes and embryos increases as development proceeds (from MII oocytes to eight-cell and eyed embryos) [22], and the value for P_{DMSO} at the eyed-embryo stage was 0.82×10^{-3} cm/min [24]. Considering that the P_s values of GV oocytes are $1.19–2.21 \times 10^{-3}$ cm/min (Table 4), GV oocytes have an advantage in cryopreservation at least in medaka. However, glycerol is not suitable for cryopreservation because the permeability of GV oocytes to glycerol was too low to be calculated, as in the case of MII oocytes.

In MII oocytes, it was shown that the chorion hinders the permeation of DMSO. However, the P_{DMSO} of intact GV oocytes ($1.19 \pm 0.01 \times 10^{-3}$ cm/min) was much higher than that of dechorionated MII oocytes ($0.14 \pm 0.01 \times 10^{-3}$ cm/min) (Table 4). This suggests that the permeability to DMSO of the plasma membrane and the chorion of GV oocytes is markedly higher than that of MII oocytes and that the permeability decreases during the final maturation period. Thus, not only the higher permeability of the plasma membrane but also the higher permeability of the chorion is also an advantage of GV oocytes for cryopreservation.

Zhang and Rawson showed much larger values for water-permeability of zebrafish embryos at the one-cell (0.34 ± 0.16 μm/min/atm) and six-somite (0.35 ± 0.15 μm/min/atm) stages [28] compared with those in other studies (0.04 0–0.100 μm/min/atm) [5,6] and those of medaka MII oocytes (0.06 ± 0.01 μm/min/atm) in this study. This large difference may be due to the presence or absence of cryoprotectants in solutions for measuring permeability to water. We, and Hagedorn et al. [6], calculated water-permeability of oocytes and embryos in solutions containing cell non-permeating solutes. On the other hand, Zhang and Rawson [28] obtained the values of L_P in the presence of methanol. In the presence of cryoprotectants, an increase in the membrane permeability parameter has been noted [18].

In this study, we have demonstrated that immature medaka oocytes have relatively high water- and cryoprotectant-permeability. But the permeability may not be sufficiently high for cryopreserving them because fish oocytes have a huge volume compared with mammalian oocytes and embryos. During the last decade, small intrinsic membrane proteins that act as water channels have been discovered and characterized [26]. These proteins, called aquaporins, occur in two groups: one subgroup is highly selective for water and the other subgroup transports not only water but also neutral solutes with a small molecular weight, such as cell-permeating cryoprotectants. We have already demonstrated that the artificial expression of aquaporin-3, which acts as a water/cryoprotectant channel, through injection of its cRNA, increases the water- and cryoprotectant-permeability of mouse oocytes [3]. We have also demonstrated that the artificial expression improves the tolerance of mouse oocytes for cryopreservation [3]. The artificial expression of aquaporin-1 also improves tolerance in yeast [25]. Aquaporin-3 can be artificially expressed in zebrafish embryos and the expression improves water- and cryoprotectant-permeability [8]. Thus, the expression of such water channels in immature fish oocytes might be effective for the cryopreservation of fish oocytes.

In conclusion, we have shown that immature oocytes are relatively permeable by water and cryoprotectant, whereas matured oocytes have quite low membrane permeability. These results suggest that, with maturation, medaka oocytes become less permeable to water and to small neutral solutes, probably by acquiring resistance to hypo-

tonic conditions before being spawned in fresh water. Since such changes would make it difficult to cryopreserve matured oocytes (and maybe embryos), immature oocytes would be more suitable for cryopreservation.

References

[1] K. Aoki, M. Okamoto, K. Tatsumi, Y. Ishikawa, Cryopreservation of medaka spermatozoa, Zool. Sci. 14 (1997) 641–644.

[2] J.C. Briggs, N. Egami, The medaka (*Oryzias latipes*). A commentary and a bibliography, J. Fish. Res. Bd. Canada 16 (1959) 363–380.

[3] K. Edashige, Y. Yamaji, F.W. Kleinhans, M. Kasai, Artificial expression of aquaporin-3 improves the survival of mouse oocytes after cryopreservation, Biol. Reprod. 68 (2003) 87–94.

[4] M. Hagedorn, E.W. Hsu, U. Pilatus, D.E. Wildt, W.F. Rall, S.J. Blackband, Magnetic resonance microscopy and spectroscopy reveal kinetics of cryoprotectant permeation in a multicompartmental biological system, Proc. Natl. Acad. Sci. USA 93 (1996) 7454–7459.

[5] M. Hagedorn, E. Hsu, F.W. Kleinhans, D.E. Wildt, New approaches for studying the permeability of fish embryos: toward successful cryopreservation, Cryobiology 34 (1997) 335–347.

[6] M. Hagedorn, F.W. Kleinhans, R. Freitas, J. Liu, E.W. Hsu, D.E. Wildt, W.F. Rall, Water distribution and permeability of zebrafish embryos, *Brachydanio rerio*, J. Exp. Zool. 278 (1997) 356–371.

[7] M. Hagedorn, F.W. Kleinhans, D. Artemov, U. Pilatus, Characterization of a major permeability barrier in the zebrafish embryo, Biol. Reprod. 59 (1998) 1240–1250.

[8] M. Hagedorn, S.L. Lance, D.M. Fonseca, F.W. Kleinhans, D. Artimov, R. Fleischer, A.T.M.S. Hoque, M.B. Hamilton, B.S. Pukazhenthi, Altering fish embryos with aquaporin-3: an essential step toward successful cryopreservation, Biol. Reprod. 67 (2002) 961–966.

[9] B. Harvey, M.J. Ashwood-Smith, Cryoprotectant penetration and supercooling in the eggs of salmonid fishes, Cryobiology 19 (1982) 29–40.

[10] B. Harvey, J.B. Chamberlain, Water permeability in the developing embryo of the zebrafish, *Brachydanio rerio*, Can. J. Zool. 60 (1982) 268–270.

[11] B. Harvey, R.N. Kelly, M.J. Ashwood-Smith, Permeability of intact and dechorionated zebra fish embryos to glycerol and dimethyl sulfoxide, Cryobiology 20 (1983) 432–439.

[12] T. Iwamatsu, S.Y. Takahashi, N. Sakai, Y. Nagahama, K. Onitake, Induction and inhibition of in vitro oocyte maturation and production of steroids in fish follicles by forskolin, J. Exp. Zool. 241 (1987) 101–111.

[13] T. Iwamatsu, R.A. Fluck, T. Mori, Mechanical dechorionation of fertilized eggs for experimental embryology in the Medaka, Zool. Sci. 10 (1993) 945–951.

[14] O. Kedem, A. Katchalsky, Thermodynamic analysis of the permeability of biological membranes to non-electrolytes, Biochim. Biophys. Acta 27 (1958) 229–246.

[15] F.W. Kleinhans, Membrane permeability modeling: Kedem–Katchalsky vs a two-parameter formalism, Cryobiology 37 (1998) 271–289.

[16] S.P. Leibo, Water permeability and its activation energy of fertilized and unfertilized mouse ova, J. Membr. Biol. 53 (1980) 179–188.

[17] C.A. Loeffler, S. Lovtrup, Water balance in the salmon egg, J. Exp. Biol. 52 (1970) 291–298.

[18] J.J. McGrath, J. Hunter, A. Bernard, B. Fuller, On the use of microdiffusion chamber methods to determine the coupled transport of water and cryoprotective agents across biological membrane, in: K.R. Diller, A. Shitger (Eds.), Macroscopic and Microscopic Heat and Mass Transfer in Biomedical Engineering, Elsevier, Amsterdam, 1992, pp. 271–296.

[19] P. Mazur, Equilibrium, quasi-equilibrium, and nonequilibrium freezing of mammalian embryos, Cell Biophys. 17 (1990) 53–92.

[20] D.M. Prescott, Effect of activation on the water permeability of salmon eggs, J. Cell. Comp. Physiol. 45 (1955) 1–12.

[21] W.F. Rall, Advances in the cryopreservation of embryos and prospects for application to the conservation of salmonid fishes, in: J.G. Cloud, G.H. Thorgaad (Eds.), Genetic Conservation of Salmonid Fishes, Plenum, New York, 1993, pp. 137–158.

[22] P. Routray, T. Suzuki, C.A. Strüssmann, R. Takai, Factors affecting the uptake of DMSO by the eggs and embryos of medaka, *Oryzias latipes*, Theriogenology 58 (2002) 1483–1496.

[23] C.A. Strüssmann, H. Nakatsugawa, F. Takashima, M. Hasobe, T. Suzuki, R. Takai, Cryopreservation of isolated fish blastomeres: effect of cell stage, cryoprotectant concentration, and cooling rate on postthawing survival, Cryobiology 39 (1999) 252–261.

[24] T. Suzuki, H. Komada, R. Takai, K. Arii, T.T. Kozima, Relation between toxicity of cryoprotectant DMSO and its concentration in several fish embryos, Fish. Sci. 61 (1995) 193–197.

[25] A. Tanghe, P. VanDijck, F. Dumortier, A. Teunissen, S. Hohmann, J.M. Thevelein, Aquaporin expression correlates with freeze tolerance in baker's yeastt, and overexpression improves freeze tolerance in industrial yeast, Appl. Environ. Microbiol. 68 (2002) 5981–5989.

[26] A.S. Verkman, A.K. Mitra, Structure and function of aquaporin water channels, Am. J. Physiol. Ren. Physiol. 278 (2000) F13–F28.

[27] A.V. Wolf, M.G. Brown, P.G. Prentiss, Concentration properties of aqueous solutions: conversion tables, in: R.C. Weast (Ed.), Handbook of Chemistry and Physics, fifty first ed., Chemical Rubber Co., Cleveland, 1970, pp. D181–D226.

[28] T. Zhang, D.M. Rawson, Permeability of dechorionated one-cell and six-somite stage zebrafish (*Brachydanio rerio*) embryos to water and methanol, Cryobiology 37 (1998) 13–21.

Development/Plasticity/Repair

Generation of Reelin-Positive Marginal Zone Cells from the Caudomedial Wall of Telencephalic Vesicles

Keiko Takiguchi-Hayashi,[1] Mariko Sekiguchi,[1] Shizuko Ashigaki,[1,3] Masako Takamatsu,[3] Hiroshi Hasegawa,[3] Rika Suzuki-Migishima,[2] Minesuke Yokoyama,[2] Shigetada Nakanishi,[4,5] and Yasuto Tanabe[1,3]

[1]Translational Research Department, Molecular Bio-Medicine Unit, [2]Mouse Genome Technology Center, and Precursory Research for Embryonic Science and Technology, Japan Science and Technology, Mitsubishi Kagaku Institute of Life Sciences, Machida, Tokyo, 194-8511, [4]Department of Biological Sciences, Faculty of Medicine, and [5]Department of Molecular and System Biology, Graduate School of Biostudies, Kyoto University, Kyoto 606-8501, Japan

An early and fundamental step of the laminar organization of developing neocortex is controlled by the developmental programs that critically depend on the activities of reelin-positive cells in the marginal zone. However, the ontogeny of reelin-positive cells remained elusive. To gain insights into the spatial and temporal regulation of reelin-positive marginal zone cell development, we used a transgenic mouse line in which we defined the green fluorescent protein (GFP) transgene as a novel reliable molecular marker of reelin-positive marginal zone cells from the early stages of their development. We further used *exo utero* electroporation-mediated gene transfer that allows us to mark progenitor cells and monitor the descendants in the telencephalon *in vivo*. We show here the generation of reelin-positive marginal zone cells from the caudomedial wall of telencephalic vesicles, including the cortical hem, where the prominent expression of GFP is initially detected. These neurons tangentially migrate at the cortical marginal zone and are distributed throughout the entire neocortex in a caudomedial-high to rostrolateral-low gradient during the dynamic developmental period of corticogenesis. Therefore, our findings on reelin-positive marginal zone cells, in addition to the cortical interneurons, add to the emerging view that the neocortex consists of neuronal subtypes that originate from a focal source extrinsic to the neocortex, migrate tangentially into the neocortex, and thereby underlie neural organization of the neocortex.

Key words: Cajal–Retzius cells; neocortex; cerebral cortex; laminar organization; tangential cell migration; caudomedial–rostrolateral axis

Introduction

In the developing neocortex, the generation of distinct classes of cortical neurons is controlled by the hierarchical series of cellular interactions that culminate in the areal and laminar organization of distinct cortical areas. After the final cell mitosis, postmitotic cortical neurons migrate in a radial direction from the ventricular zone (VZ), form a cortical plate (CP), and subdivide the preexisting preplate into the superficial marginal zone (MZ) and the deeper subplate (Gupta et al., 2002; Nadarajah and Parnavelas, 2002). reelin-positive cells (Meyer et al., 1999) are one of the major neuronal subtypes located in the MZ and are distributed evenly throughout the entire cerebral cortex in a wide variety of mammalian species (Marín-Padilla, 1998; Supèr et al., 1998). The analyses of *reeler* mutant mice (Ogawa et al., 1995; Meyer et al., 1999; Rice and Curran, 2001; Tissir and Goffinet, 2003), together with studies in human congenital lissencephaly (Gleeson and Walsh, 2000), led to the suggestion that the neocortical neural organization depends on the activities of reelin-positive cells that govern the laminar arrangements of CP cells from the early stages of development. Studies on how reelin-positive cell generation is spatially and temporally controlled in the telencephalon might, therefore, provide a solid cellular framework for understanding neural organization during development of the neocortex.

Despite many advances in the characterization of the way CP neurons are generated and organized into distinct layers (Gupta et al., 2002; Nadarajah and Parnavelas, 2002), the ontogeny of reelin-positive cells has remained elusive. The concept of a dual origin of the cerebral cortex, together with the classical concept from the time of Ramón y Cajal, provided a prevailing view that both reelin-positive cells and subplate are generated as preplate from the underlying VZ before the formation of CP (Marín-Padilla, 1978, 1998). Consistent with these ideas, several studies suggest the local generation of reelin-positive cells within the neocortical area (Meyer et al., 2000; Hevner et al., 2003). In contrast, several lines of evidence suggest that neocortical reelin-positive cells may originate from locations extrinsic to the neocortex (Meyer et al., 1998, 2002; Lavdas et al., 1999; Shinozaki et al., 2002). Together, these studies raised the possibility that neo-

Received Oct. 16, 2003; revised Dec. 28, 2003; accepted Jan. 6, 2004.

This work was supported by grants from Precursory Research for Embryonic Science and Technology in Japan Science and Technology (to Y.T.). We thank S. Kamijyo, M. Matsuo, T. Akiyama, N. Iizawa, T. Hino, and M. Takabe at Mitsubishi Kagaku Institute of Life Sciences Mouse Facility for their assistance. We also thank N. Osumi at Tohoku University for anti-Pax6 antibody, S. Yasugi and K. Fukuda at Tokyo Metropolitan University, K. Tamura at Tohoku University, and R. Kageyama and H. Yamazaki at Kyoto University for their kind advice in ISH technique, K. Arishima and T. Takizawa at Azabu University and H. Ohtani and T. Hatta at Simane Medical University for their kind advice on mouse surgery, S. C. Fujita at MITILS for anti-GFP antibody (Ab), Y. Yamakuni at MITILS for anti-calbindin Ab, N. Sugou at Osaka University for mouse *Tbr1*, Y. Hatanaka at Osaka University for *pCAGGS-EGFP*, I. Saitou at University of Tokyo for *pCAGGS-LacZ*, J. Miyazaki at Osaka University for *pCAGGs*, and S. Arber at University of Basel for *NLS-LacZ*. Y.T. thanks Dr. Watanabe at Kyoto University for the initial collaborative work. We thank S. Narita, A. Kudo, S. Nishimiya, and Y. Tsunekawa for their technical support. We are grateful to S. Goto, M. Setou, and T. Takeuchi at MITILS and T. M. Jessell at Columbia University for their thoughtful comments on a previous version of this manuscript.

Correspondence should be addressed to Dr. Yasuto Tanabe, 11 Minami-Ooya, Machida, Tokyo, 194-8511, Japan. E-mail: ytanabe@libra.ls.m-kagaku.co.jp.

DOI:10.1523/JNEUROSCI.4671-03.2004

 0270-6474/04/242286-10$15.00/0

cortical reelin-positive cells consist of heterogeneous cell groups that are generated at varied locations in the telencephalon, both extrinsic and intrinsic to the neocortex (Meyer et al., 2002). However, there is no direct evidence for those cells that have been generated at the putative sources to comprise reelin-positive cells located in the MZ of the neocortex. Moreover, the extent to which prospective reelin-positive cells from distinct sources contribute within the entire population of reelin-positive cells remains obscure. In addition, the way in which prospective reelin-positive cells from distinct sources are distributed throughout the entire cerebral cortical MZ remains to be defined *in vivo*. We show here prospective reelin-positive cells are generated from the caudomedial wall of telencephalic vesicles (CMWT) and exhibit the extensive tangential migration throughout the neocortical MZ in a caudomedial–rostrolateral cellular gradient.

Materials and Methods

Mice. C57BL/6 *Tg* mice (Watanabe et al., 1998) and ICR Jcl mice (CLEA Japan, Inc., Tokyo, Japan) were used for the experiments. Each strain was mated to obtain offsprings in house in an environmentally controlled room under the Guidelines for Use of Laboratory Animals (Japan Neuroscience Society) and the Animal Care and Use Committee (Mitsubishi Kagaku Institute of Life Sciences). Noon of the date on which the vaginal plug was detected in the morning was designated as embryonic day (E) 0.5.

Immunohistochemistry and in situ *hybridization.* Embryos were fixed by cardiac perfusion with 4% paraformaldehyde (PFA), 7% picric acid in 0.1 M sodium phosphate buffer, pH 7.4, for immunohistochemistry (IH), and with 4% PFA in 0.1 M sodium phosphate buffer, pH 7.4, for *in situ* hybridization (ISH). The brain was postfixed in the fixative for 2 hr for IH and for overnight for ISH. Samples were then equilibrated in 25% of sucrose in PBS and embedded in OCT compound (Sakura, Tokyo, Japan). Frozen sections were cut with a cryostat (MICROM HM500OM; Carl Zeiss, Oberkochen, Germany) at 10 μm and mounted onto MAS-coated glass slides (Matsunami, Osaka, Japan).

Immunohistochemical staining was performed as described (Takiguchi-Hayashi et al., 1998). Primary antibodies (Abs) used were: polyclonal rabbit anti-βgalactosidase Ab (Cappel, Worthington, PA) in 1:1000; monoclonal rat anti-GFP (JFP-K2, kindly provided by Dr. S. C. Fujita) supernatant, polyclonal rabbit anti-calbindin Ab (spot 35, kindly provided by Dr. T. Yamakuni) in 1:1000, polyclonal rabbit anti-calretinin Ab (Chemicon, Temecula, CA) in 1:1000, polyclonal rabbit anti-Pax6 Ab (kindly provided by Dr. N. Osumi) in 1:1000. Secondary Abs used were FITC-conjugated goat anti-rat IgG (AP183F; Chemicon) in 1:100, and cyanine3 (Cy3)-conjugated anti rabbit IgG (Jackson ImmunoResearch, West Grove, PA) in 1:400.

RNA probes prepared were *EGFP* (kindly provided by Dr. Watanabe), *reelin* (*Eco*RI/*Xho*I 1100bp fragment), *p73* (XM 131858; GenBank, 1503–2232 nucleotides), and *Lhx6* (AJ000337; GenBank, 6–651 nucleotides), *Tbr1* (U49251; GenBank, 2951–3780 nucleotides), and *Emx2* (AY117415; GenBank, 1385–1904 nucleotides). ISH was performed as described (Schaeren-Wiemers and Gerfin-Moser, 1993; Ishibashi et al., 1995) with minor modifications. For double-ISH, digoxygenin-UTP, and fluorescein-UTP (Roche Products, Hertforshire, UK) were used for labeling of the probes, and hybridization was performed simultaneously according to the procedures described in the manufacturer's protocol (TSA Biotin system; PerkinElmer Life Sciences, Emeryville, CA).

Axiovert 200M (Carl Zeiss, Jena, Germany), Olympus BX61 with a CCD camera DP50 (Olympus, Tokyo, Japan), and LSM5 PASCAL confocal microscope (Carl Zeiss) were used to obtain fluorescent images. The images were processed using Photoshop software (Adobe Systems, San Jose, CA).

X-gal staining. Embryos were fixed by cardiac perfusion with PBS containing 1% of formaldehyde, 0.2% of glutaraldehyde, and 0.02% of NP-40 for 2 hr. X-gal staining procedures for whole-mount brain or frozen sections were performed as described (Motoyama et al., 1997).

BrdU labeling study. For birth date studies, timed-pregnant *Tg* mice to which *in vitro* fertilized eggs were transferred *in utero* were injected intraperitoneally three times in 3 hr intervals with BrdU (Roche; 5 mg/ml in sterile saline) at 50 mg/kg body weight on several stages of pregnancy. The date of injections was set at ages of E10.5 ($n = 3$), E11.5 ($n = 3$), E12.5 ($n = 2$), and E13.5 ($n = 3$). The pregnant mice were maintained for several days afterwards to obtain the embryos aged at E18.5, when the embryos were processed for IH. Sections were first autoclaved at 110°C for 10 min in 0.1 M sodium citrate buffer, pH 6.0, as described (Imam et al., 1995). BrdU and GFP were detected using anti-BrdU Ab (Dako, Carpinteria, CA) and anti-GFP Ab as described (Arimatsu et al., 1999). All the nuclei of BrdU-labeled cells, including both heavily and lightly labeled cells, were counted for the analysis.

Exo utero *electroporation.* cDNA fragments of *NLS-LacZ* (kindly provided by Dr. S. Arber) were subcloned into the *pCAGGs* vector (kindly provided by Dr. J. Miyazaki). *pCAGGS-EGFP* (kindly provided by Dr. Y. Hatanaka) and *pCAGGS-LacZ* (kindly provided by Dr. I. Saitou) were also used. *Exo utero* surgery was followed as described (Muneoka et al., 1986a,b; Ngo-Muller and Muneoka, 2000) with modifications.

We prepared embryos in *exo utero* condition to transfer genes more reliably to the focal region by electroporation. Timed pregnant mice at E11.5 were deeply anesthetized with sodium pentobarbital (Nembutal; Abbott, North Chicago, IL) at 50 mg/kg body weight. A midline abdominal incision was made on the pregnant mouse, and then both horns of uterus were exposed. The number of embryos in each horn was recorded, and then three embryos in each horn were selected, and the rest of the embryos were removed from the horns of the uterus to obtain enough space for the subsequent electroporation procedures. The selected three embryos were released from the constraints of myometrium by making a longitudinal incision in the uterine myometrium at a position opposite to the side of the placenta. The myometrium contracted to the base of the placenta, and the embryos covered with their thin extraembryonic membranes were exposed. DNA solutions (5 mg/ml in 10 mM Tris-HCl, pH 8.0, with 0.016% Trypan Blue to permit visualization of injected solution in the embryos) were injected into the left side of the lateral ventricle of E11.5 telencephalon with a glass micropipette. After the injection, the embryos covered with the extraembryonic membranes were held with the tweezer-type electrode with discs of 3 mm in diameter at the tip (CUY650P3; Nepa Gene Company, Chiba, Japan). Electronic pulses of 25 V were charged five times at 950 msec intervals using a square-pulse electroporator (CUY21EDIT; Nepa Gene Company). For the electroporation aiming for the CMWT-directed gene transfer, the anode was positioned caudomedially so that the DNA is incorporated into the VZ cells of the CMWT. Likewise, the anode was always positioned on the direction to which the electroporation was conducted (see supplemental Figs. 2–4, available at www.jneurosci.org). After the procedures, embryos were placed back into the abdominal cavity of the pregnant mouse without sewing the uterine wall. The abdominal cavity was filled with prewarmed HBSS (Invitrogen, Gaithersburg, MD). Then, the abdominal wall was sewed with surgical sutures, and the skin was sewed with Autoclip applier (MikRon, Sparks, MD) to allow the embryos to develop. The pregnant mice were maintained for several days, and the embryos at E12.5–E18.5 were subjected to the analyses.

The focal restriction of electroporation-mediated gene transfer and its reproducibility was confirmed by the series of experiments shown in supplemental Figures 2–4 (available at www.jneurosci.org). For example, LacZ electroporation at E11.5 aimed for the CMWT was conducted in 12 embryos in total, among which eight embryos survived until E12.5, and all the eight embryos exhibited the focal restriction of gene transfer at the CMWT. In addition, when we analyzed 11 anterior-pole electroporated samples, 3 lateral wall electroporated samples, and 9 CMWT electroporated samples of E14.5 embryos, all the electroporated samples exhibited the focal LacZ expression in the ventricular zone adjacent to the electroporated region (see Fig. 4).

Slice cultures. Brains were embedded in 4% low-melting agarose gel, and 300-μm-thick parasagittal or oblique sections were cut on a vibratome, as shown in Figure 7I. Slices were then transferred to collagen-coated culture membranes (Millicell-CM; 30 mm in diameter, 0.4 μm pore size; Millipore, Bedford, MA) in organ tissue culture dishes containing 1.3 ml of medium (Invitrogen; MEM-F-12 with glutamine, 5% PNCS, 5% horse serum, penicillin, and streptomycin) as described (Ari-

matsu et al., 1992). They were subsequently cultured for several hours in sterile condition in an incubator (5% CO_2, at 37°C), after which the medium was changed to Neurobasal/B-27 (Invitrogen). During the culture period, images of GFP fluorescent were captured by AxioCam MRm CCD camera with Zeiss Stemi SVII microscope (Carl Zeiss) at appropriate time intervals.

Results

Embryonic reelin-positive cells at the neocortical marginal zone are marked by GFP expression

Our study in *IG17* transgenic mice (*Tg* mice) (Watanabe et al., 1998) revealed that the membrane-anchored *GFP* transgene is specifically expressed by reelin-positive cells in the MZ during the early postnatal period (Soda et al., 2003). This observation prompted us to examine whether the *GFP* transgene can be used as a novel marker for the embryonic reelin-positive cells and to analyze the ontogeny of reelin-positive marginal zone cells in the early embryonic stages of neocortical development. We first examined whether embryonic GFP expression is restricted to the reelin-positive cells in *Tg* mouse telencephalon. Murine embryonic reelin-positive cells can be characterized by the uniform location of cell bodies in the MZ, neurite extensions in a tangential direction, and the early onset of generation compared with the CP neurons (Supèr et al., 1998). We analyzed the telencephalon of *Tg* mouse embryos from E14.5 onward, by which time the neocortical MZ has emerged, and reelin-positive cells have acquired their characteristic identities (Wood et al., 1992; Polleux et al., 1997).

We first defined the pattern of GFP expression in *Tg* mouse telencephalon. At E14.5, GFP expression was detected in the MZ of all the rostrocaudal levels of the cerebral cortex (Fig. 1*a–c*). Intensive GFP expression in the MZ encompassed nearly the entire cerebral cortex, including the neocortex, the piriform, the cingulate cortex (Fig. 1*a–c*), and the dorsal and ventral regions adjacent to the choroid plexus (Fig. 1*b,c*). From E16.5 onward, although the MZ itself was expanded, the pattern of GFP expression remained essentially similar and persisted until the latest age examined (E18.5) (Fig.1*e,f*) (data not shown). GFP-expressing cell bodies were embedded in tangentially oriented intricate nerve fibers in the MZ (Fig. 1*d–f*).

We next analyzed the pattern of GFP expression within the neocortical MZ in relation to the molecular markers that have been used to define the major types of MZ cells, including the reelin-positive cells. Reelin and p73 serve as reliable markers of reelin-positive cells from the early stages of their development (Schiffmann et al., 1997; Alcantara et al., 1998; Meyer et al., 2002). Lhx6 marks other neuronal subtypes in the murine neocortical MZ (Lavdas et al., 1999). Double *in situ* analyses of *GFP* with *reelin* at E14.5–18.5 revealed that virtually all the *GFP*-positive cells located at the neocortex coexpressed *reelin*, and vice versa (Fig. 1*g–i*) (data not shown). Similarly, virtually all the *GFP*-positive cells were colabeled by *p73* in the neocortical MZ at E14.5–18.5 (Fig. 1*j–l*) (data not shown). On the contrary, the double *in situ* analyses of *GFP* in relation to *Lhx6* revealed that, at E14.5, the expression of *GFP* and *Lhx6* was mutually exclusive in the neocortical MZ (Fig. 1*m–o*). Double *in situ* hybridization of *Emx2* and *Tbr1* in relation to *GFP* revealed that the expression of *Emx2* and *Tbr1* was evident in virtually all of the *GFP*-positive cells in the marginal zone of the neocortex at E14.5 (supplemental Fig. 1, available at www.jneurosci.org). Confocal microscopic analyses of double immunostaining of Pax6 in relation to GFP revealed that Pax6 expression was evident in some of the GFP-positive cells in the marginal zone of E14.5 neocortex. Previous studies show that most of the reelin-positive marginal zone cells at E14.5 express Emx2, and Tbr1, and some of them express Pax6 (Stoykova et al., 2003). Confocal microscopy studies of calretinin in relation to GFP revealed that calretinin expression was evident at E14.5 in most of the GFP-expressing cells in the marginal zone of the neocortex, but a few GFP expressing cells were negative for the calretinin expression (supplemental Fig. 1, available at www.jneurosci.org). From E16.5 onward, however, there was a nearly complete overlap of GFP and calretinin expression in the marginal zone of neocortex (data not shown). These temporal expression profiles of GFP in relation to calretinin are consistent with the idea that the onset of GFP expression is before that of calretinin. Taking into account of fact that the onset of reelin expression also precedes that of calretinin in reelin-positive marginal zone cells, these data further support the notion that the expression pattern of GFP coincides with that of reelin in the *Tg* neocortex. Calbindin defines mostly non-reelin-positive cells at E14.5 cerebral cortical marginal zone. Consistent with this, nearly all of the calbindin staining was not detected in GFP-expressing cells in the neocortical marginal zone of E14.5 *Tg* mouse embryos (supplemental Fig. 1, available at www.jneurosci.org).

Together, these findings provide evidence that, at the neocortex, GFP is expressed exclusively by reelin-positive cells in the embryonic *Tg* telencephalon from E14.5 onward. These data

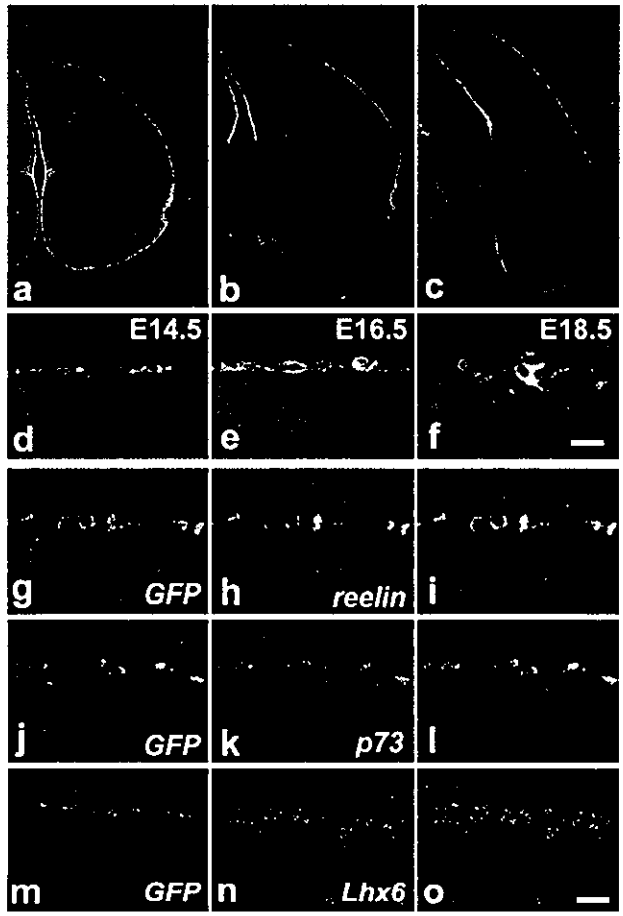

Figure 1. Expression of GFP by reelin-positive cells at the neocortex of *Tg* mouse embryos. *a–c*, Coronal sections at the anterior (*a*), intermediate (*b*), and posterior (*c*) levels of E14.5 cerebral cortex showing the restricted expression of GFP in the entire MZ. *d–f*, Restriction of GFP in the neocortical MZ at E14.5 (*d*), E16.5 (*e*), and E18.5 (*f*). *g–o*, Double ISH analyses of *GFP* in green (*g, i, j, l, m, o*) with *reelin* in red (*h, i*), *p73* in red (*k, l*), and *Lhx6* in red (*n, o*) of the E14.5 neocortical MZ. Scale bars, 20 μm.

demonstrate that GFP, in addition to reelin and p73, serves as another reliable molecular marker of reelin-positive cell identity in the embryonic *Tg* neocortical MZ.

Birth date analyses of GFP-expressing cells at the neocortical MZ

To substantiate the notion that *GFP* transgene at the neocortex marks reelin-positive cells exclusively, we examined the birth date of GFP-positive cells in the MZ by 5′-bromo-2′ deoxyuridine (BrdU) labeling studies. Progenitor cells at S-phase of the cell cycle were labeled *in vivo* by injecting BrdU into pregnant mice from E10.5 onward, and the BrdU-labeled GFP-positive cells were subjected to the immunocytochemical analyses at E18.5 (Fig. 2*a–c*). More than 90% of GFP-positive cells in the neocortical MZ were colabeled with BrdU that was injected at E10.5, indicating nearly all of the GFP-positive cells are generated from E10.5 onward (Fig. 2*a*, supplemental Table 1, available at www.jneurosci.org). The proportion declined as the date of injection was set at later embryonic ages and became <4% at injection date of E13.5. These data indicate that ~53% of GFP-positive neocortical MZ cells were generated at E10.5–11.5, ~ 29% at E11.5–12.5, ~ 8% at E12.5–13.5, and the rest before E10.5 and/or after E13.5 (Fig. 2*b*; see also supplemental Table 1, available at www.jneurosci.org). It appears there was no regional difference in the neocortex along the dorsolateral axis for the temporal pattern of generation of GFP-positive cells (Fig. 2*a*). Previous studies dealing with the issue of timing of reelin-positive cell generation were able to show that most of the reelin-positive cells were generated at approximately E10.5–E12.5 in the murine telencephalon (Wood et al., 1992; Hevner et al., 2003). Thus, our BrdU labeling studies are consistent with the idea that, in the neocortex, *GFP* transgene is expressed exclusively by reelin-positive cells. Importantly, the fact that 40.3% of reelin-positive cells on average were generated from E11.5 onward (supplemental Table 1, available at www.jneurosci.org) allowed us to examine the origins of reelin-positive cells by using electroporation-mediated gene transfer method at E11.5 (see below).

Onset of GFP expression in relation to reelin and p73

To begin to address the issue of ontogeny of reelin-positive cells, we examined the onset of expression of *GFP* in relation to those of *reelin* and *p73* in *Tg* mouse telencephalon (Fig. 3). Based on our BrdU labeling studies, we focused our analysis on E10.5–E11.5 when most of the reelin-positive cells were generated. We asked if the expression of *GFP* transgene could be detected before that of *reelin* or *p73*, and the *GFP* transgene might serve as a tool to monitor the onset of reelin-positive cell generation.

At E10.5, prominent expression of *GFP* was first detected at the ventral region of CMWT at the rostrocaudal level where the telencephalon–diencephalon junction (TDJ) exists, merging apparently with the *GFP* expression at the diencephalon (Fig. 3*b,f*). *GFP* expression was detected in continuity at the subpial layer of ventral subpallium (Fig. 3*b*), including the GE primordium (Fig. 3*d,e*). Some GFP-positive cells were scattered in the VZ at these locations, suggesting their local generation (Fig. 3*b,d–f*, arrows). In addition, a few GFP-positive cells were detected at the subpial layer of the prospective neocortex (Fig. 3*b,d*, arrowhead). In contrast, *p73* expression was detected at the dorsal region of CMWT and extended into the prospective neocortical areas (Fig. 3*a*, arrowheads). Some p73-expressing cells were detected even in the VZ of the CMWT (Fig. 3*a*, arrows) (Meyer et al., 2002). A few, if any, *p73*, *GFP*, and *reelin*-positive cells were also scattered in the VZ of the neocortical primordium (Fig. 3*a*, data not shown).

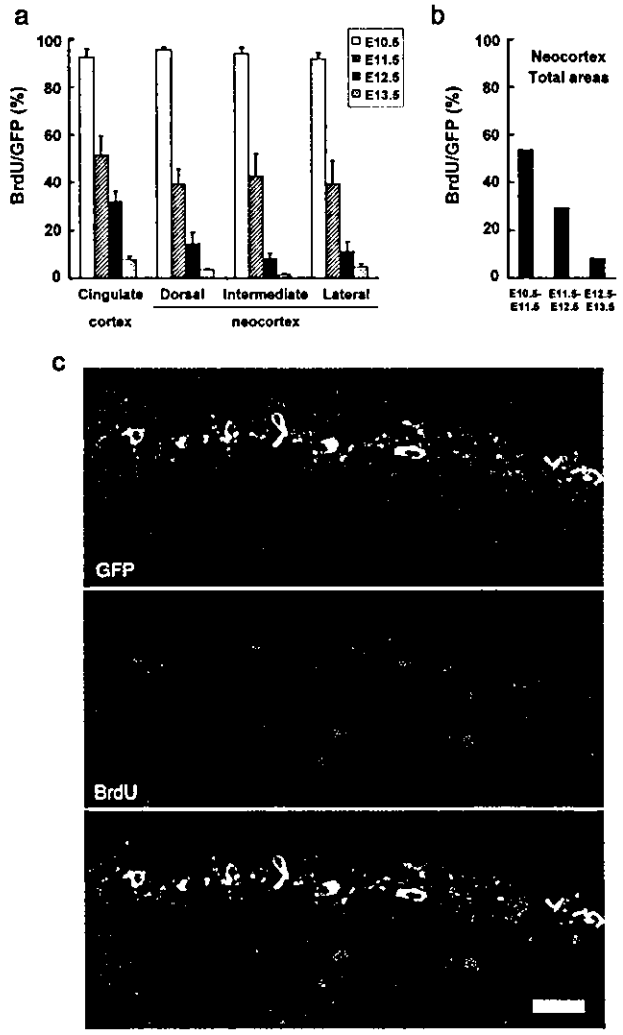

Figure 2. Birth date analyses of GFP-positive cells in the cerebral cortical MZ by the BrdU labeling study. *a*, Quantitative analyses of the proportion of the number of BrdU and GFP coexpressing cells in the total number of GFP-expressing cells in E18.5 cerebral cortical MZ. Data points represent mean values ± SE from >160 cells. Neocortical MZ was divided into three areas along the dorsolateral axis. There was no significant regional difference in the generation of GFP-positive cells among the three regions. The temporal pattern of generation of GFP-positive cells at the cingulate cortex was similar to that of neocortex. All the BrdU-labeled cells, including both the heavily labeled and weakly labeled cells, were counted for the analyses. *b*, Summary of quantitative analyses of birth date of GFP-positive cells in the entire neocortical MZ. Data represent the proportion of the number of GFP-positive cells that are generated at each of the time windows. See supplemental Table 1 (available at www.jneurosci.org) for the detailed results of quantitative analyses. The percentage of GFP-positive cells generated in the three distinct regions of neocortex from E10.5 onward was 93.3% on average; the percentage of GFP-positive cells generated from E11.5 onward was 40.3% on average; the percentage of GFP-positive cells generated from E12.5 onward was 11.3% on average, the percentage of GFP-positive cells generated from E13.5 onward was 3.2% on average. By subtracting these numbers, we obtain, for example, 53% for the percentage of GFP-positive cells that are generated between E10.5 and E11.5 intervals. *c*, A representative coronal section showing the staining patterns of GFP and BrdU. A few number of GFP-, BrdU-double positive cells are shown. Scale bar, 20 μm.

At E11.5, the area of prominent *GFP* expression in the CMWT adjacent to the TDJ expanded in a bifurcated stream of cells (Fig. 3*h,k*). It extended in both dorsal and ventral directions at the subpial layer of telencephalic vesicles: dorsally along the dorsal medial wall of telencephalon (Fig. 3*h,k*, arrowheads), and ventrally along the ventral subpallium (Fig. 3*h,k*, arrows). The expression of *GFP* at the ventral subpallium appeared to be followed by *reelin* expression, and accordingly, the area of *reelin*

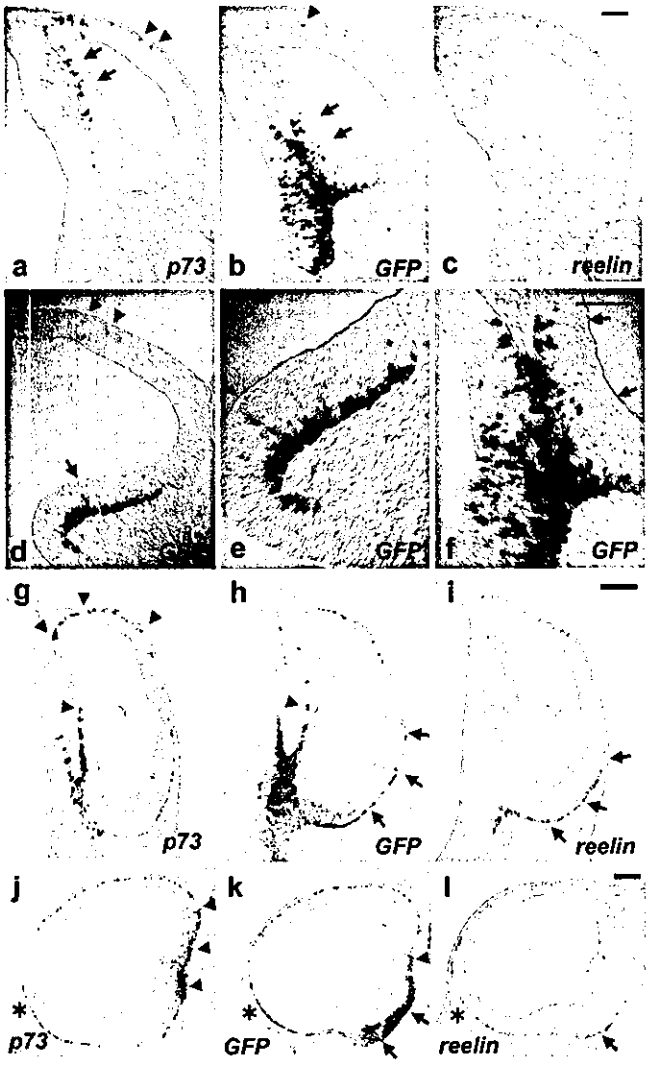

Figure 3. Onsets of *p73*, *GFP*, and *reelin* expression in the telencephalon. ISH analyses of *p73* (*a*, *g*, *j*), *GFP* (*b*, *d–f*, *h*, *k*), and *reelin* (*c*, *i*, *l*) at E10.5 (*a–f*) and at E11.5 (*g–l*). Coronal sections of telencephalon at the rostrocaudal level where the TDJ exists (*a–c*, *f–i*), coronal sections at the rostrocaudal level where the GE primordium exists (*d*, *e*), and parasagittal sections through the CMWT (*j–l*) are shown. *e*, *f*, High-power views of *d* and *b*, respectively. Rostral is to the left in *j–l*. Arrows in *a*, *b*, *d*, *e*, and *f* show the VZ staining. Arrowheads in *a*, *b*, and *d* show staining at the subpial layer of prospective neocortex. Arrowheads in *g*, *h*, *j*, and *k* show gene expression at the dorsal part, whereas arrows in *h*, *i*, *k*, and *l* show gene expression at the ventral part of cerebral cortex. Scale bars: *a–f*, 100 μm; *g–l*, 200 μm.

expression appeared to be contained within a broader area of *GFP* expression (Fig. 3*h*,*i*,*k*,*l*, arrows). Moreover, there was a graded distribution of *GFP* and *reelin* expression from ventral to lateral at the subpial layer of cerebral cortex (Fig. 3*h*,*i*, arrows). Conversely, the expression of *p73* at the dorsal region of CMWT appeared to be followed by that of *GFP* (Fig. 3*g*,*h*,*j*,*k*, arrowheads). In contrast to the *GFP* and *reelin* expression pattern, *p73* expression was distributed in a dorsal to lateral gradient at the subpial layer and appeared to emanate from the dorsal region of CMWT (Fig. 3*g*,*j*, arrows). *p73*, *GFP*, and *reelin* expressions were detected on the ventral cortical surface near the olfactory primordium (Fig. 3*j–l*, asterisks) (Meyer et al., 1998). By E12.5, all three genes were detected uniformly in the MZ of the cerebral cortex (data not shown).

Together, these results show the CMWT adjacent to TDJ is the region where most prominent expression of *GFP* is detected (Fig. 3*b*,*f*,*h*,*k*). Importantly, the expression of *GFP* at this locus was temporally overlapped with that of *p73* (Fig. 3*a*,*g*,*j*) and *reelin* (Fig. 3*c*,*i*,*l*). At the ventral region of CMWT, the onset of expression of *GFP* appeared to precede those of *reelin* and *p73*, whereas, at the dorsal region of CMWT, the onset of expression of *p73* appeared to precede those of *GFP* and *reelin* (Fig. 3*a–c*, *g–l*). In contrast, the expression of reelin-positive cell markers in other telencephalic regions was relatively weak compared with the CMWT (Fig. 3*a–d*, *g–l*). In summary, over the major period of reelin-positive cell generation, the prominent expressions of *GFP*, *reelin*, and *p73* appeared to emanate from the CMWT into the neocortex. Therefore, these observations raised the possibility that the CMWT is a site where prospective CR cells are generated.

Generation of prospective reelin-positive cells at the CMWT

To establish a direct link between the cells generated at the CMWT and reelin-positive marginal zone cells at the neocortex *in vivo*, we used *exo utero* electroporation-mediated gene transfer to mark VZ cells at the CMWT by *LacZ* and to follow the LacZ-labeled descendants. We focused our analysis on reelin-positive cells generated at E11.5, because the electroporation-mediated gene transfer can be carried out reliably and reproducibly onto the focal region under a microscope from E11.5 onward (supplemental Figs. 2–4, available at www.jneurosci.org). Plasmid DNA injection into the E10.5 embryonic telencephalic vesicles *exo utero* was hampered by the presence of deciduas surrounding the embryos, and the survival rate of embryos severely decreased by removing deciduas.

We first electroporated *LacZ* into cells located at the anterior pole (Fig. 4*a*,*e*,*h*) or the lateral wall (Fig. 4*c*,*f*,*i*) of telencephalic vesicles at E11.5, permitted embryos to develop until E14.5, and analyzed the LacZ expression pattern. Most of the LacZ-positive descendants essentially remained at the neighboring regions where the electroporation-mediated gene transfer was conducted (Fig. 4*a*,*c*). The LacZ expression was confined, mostly to the VZ (Fig. 4*e*,*f*, arrows) and the CP, but barely, if any, to the MZ of the neocortex (Fig. 4*e*,*f*,*h*,*i*). In contrast, when we electroporated *LacZ* into cells located at the CMWT at E11.5, a population of LacZ-positive descendants was detected on nearly the entire cortical surface in a caudomedial-high to rostrolateral-low gradient at E14.5 (Fig. 4*b*,*d*). Coronal sections revealed intensive LacZ staining in the MZ throughout the entire dorsoventral axis of the cerebral cortex (Fig. 4*g*,*j*). The VZ staining of LacZ was confined to the CMWT, which is consistent with the procedures of caudomedially directed electroporation of gene transfer (Fig. 4*g*, arrows). No staining was detected in the CP, the subventricular or the VZ of any other regions of the telencephalon (Fig. 4*g*,*j*).

We then examined the identity of CMWT-derived LacZ-positive descendants located in the MZ of the neocortex. We analyzed LacZ-positive cells with anti-GFP antibody at E14.5 after the electroporation of *LacZ* at E11.5 mouse (Fig. 4*k–m*). All the LacZ-positive cells detected in the MZ of the neocortex coexpressed GFP, indicating LacZ derivatives in the neocortex from the CMWT were solely reelin-positive cells. Moreover, these LacZ-positive cells appeared to form a substantial population of reelin-positive cells, especially at the posterior neocortex (Fig. 4*b*,*d*).

Together, these findings indicate that virtually all of descendants derived from the CMWT at E11.5 comprise reelin-positive cells that were distributed widely in a caudomedial-rostrolateral gradient in the cerebral cortex at E14.5. Moreover, the other regions of telencephalon, including the neocortical primordium, where the electroporation was conducted appeared to give rise to a few, if any, reelin-positive cells at E11.5.

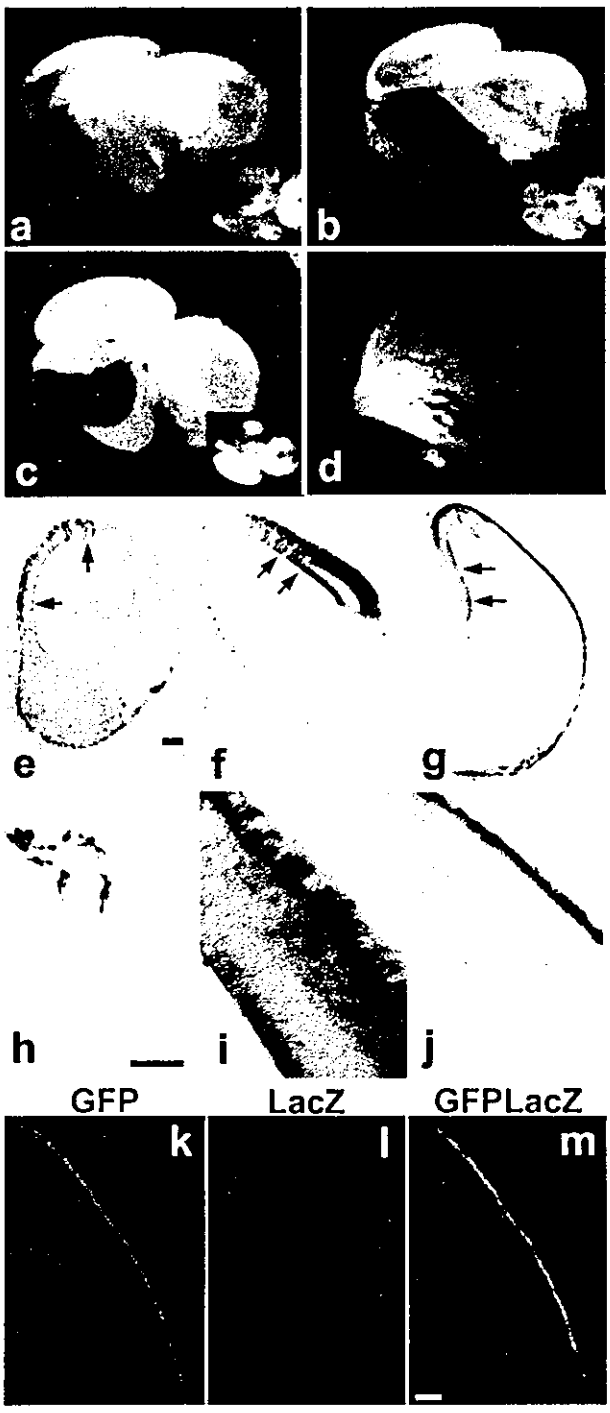

Figure 4. Generation and distribution of prospective reelin-positive cells derived from the CMWT. *a–d*, LacZ staining of E14.5 brains in whole-mount views. Electroporation was done into cells located at the anterior-pole (*a*), the lateral wall (*c*), or the caudomedial wall (*b*, *d*) of telencephalic vesicles. Inset (*a–c*), A ventral view. *d*, A lateral view shown in *b*. *e–j*, Coronal sections of E14.5 brain showing the pattern of LacZ staining. Images shown in *e* and *h* are obtained from the brain shown in *a*; *f* and *i* from *c*; *g* and *j* from *b*. Arrows (*e–g*) show the LacZ staining in the VZ. *h–j*, High-power views of *e*, *f*, and *g*, respectively, showing the neocortical areas. Electroporation into the anterior-pole sometimes resulted in the LacZ distribution in the ventral cortical MZ (*a*, *e*). Electroporation toward the CMWT exhibited only a faint, but significant, expression of LacZ at the invaginated medial wall (arrows in *g*), because of the LacZ staining has been performed in whole-mount preparation. Images are representative of 11 electroporated samples in *a*, *e*, and *h*, three electroporated samples in *c*, *f*, and *i*, and 9 electroporated samples in *b*, *d*, *g*, and *j*. Analyses of reproducibility of focal restriction of electroporation-mediated gene transfer at E14.5 revealed that all the electroporated samples exhibited the focal LacZ expression in the ventricular zone adjacent to the electroporated region. *k–m*, Double immunohistochemical analyses of GFP staining in green (*k*, *m*) and LacZ staining in red (*l*, *m*). Scale bars: *e–j*, 100 μm; *k–m*, 50 μm.

Figure 5. Origins and migratory routes of LacZ descendants at the CMWT. *a–c*, LacZ staining of coronal sections of E12.5 telencephalon at the level where CP_P reside (*a–c*). Arrows point the CP_P. Images are representative of eight electroporated samples *d–i*. NLS-LacZ staining of serial coronal sections of E14.5 telencephalon from rostral to caudal levels (*d–i*). Images are representative of five electroporated samples. Arrowheads in *d–i* show the VZ staining. Scale bars, 200 μm.

Origins and migratory pathways of prospective reelin-positive cells at the CMWT

The persistence of LacZ staining in the VZ where the electroporation was conducted led us to examine the origins at the CMWT. The LacZ staining was performed on coronal sections of the telencephalon at E12.5 after the electroporation of LacZ into the CMWT at E11.5 (Fig. 5*a–c*). In all sections examined, the NLS-LacZ staining in the MZ of the cerebral cortex was always correlated with the NLS-LacZ staining in the VZ of the CMWT region that most likely corresponded to the cortical hem. The cortical hem is characterized by its unique positions relative to the choroid plexus primordium (CP_P) (Grove et al., 1998). At the more rostral level of cerebral cortex, the LacZ expression in the MZ of the dorsal cerebral cortex was always detected together with the ventricular LacZ expression dorsal to the CP_P, corresponding to the dorsal cortical hem ($n = 8$ independent electroporated embryos) (Fig. 5*a–c*) (Grove et al., 1998). In contrast, at the more caudal level of cerebral cortex where the cortical hem can be detected both dorsal and ventral to the CP_P, LacZ expression in the MZ of the ventral cerebral cortex was always detected together with the ventricular LacZ expression ventral to the CP_P, corresponding to the ventral cortical hem ($n = 8$ independent electroporated embryos) (Fig. 5*a–c*). When either of these ventricular regions was negative for the LacZ staining, no staining was detected in the neighboring MZ (Fig. 5*a*,*c*).

Thus, the detailed analyses of the CMWT for the LacZ expres-

sion pattern after 24 hr of electroporation suggest that the cortical hem contributes to the generation of reelin-positive cells. Furthermore, these results obtained from the short time point after electroporation revealed the correlation between the origins and the direction of the initial pathways taken by the descendants. It appears that distinct pathways are taken initially by the prospective reelin-positive cells depending on the originated regions of the cortical hem. The prospective reelin-positive cells appear to take a dorsal route from the dorsal cortical hem, whereas a ventral route from the ventral cortical hem. We do not rule out the possibility, however, that CMWT regions outside of the cortical hem may also contribute to the generation of prospective reelin-positive cells.

This type of analysis also provided information on the extent of tangential migration of descendants that were derived from the cortical hem. To monitor the extent of tangential migration of descendants in the MZ of the cerebral cortex more precisely, we electroporated nuclear-localizing signals containing *LacZ* (*NLS-LacZ*) at E11.5 to detect gene-incorporated cells and monitored NLS-LacZ expression pattern at E14.5. NLS-LacZ-positive descendants detected at E14.5 cerebral cortex covered most of the cerebral cortical MZ, including the cingulate cortex, the neocortex, the piriform, and the amygdala, with caudomedial-high to rostrolateral-low graded distribution ($n = 5$ independent electroporated embryos) (Fig. 5*d–i*). The NLS-LacZ staining in the VZ of the cerebral cortex was again detected at a region of the CMWT, which corresponded to the dorsal and posterior end of cortical hem (Fig. 5*d–i*). In addition, NLS-LacZ expression in the VZ was not detected in any other regions of the cerebral cortex. Thus, these results provide additional supportive evidence that the telencephalic neuroepithelium adjacent to the choroid plexus at the CMWT, cortical hem, have contributed to the generation of prospective reelin-positive cells. Moreover, these studies suggest that reelin-positive cells that are derived from the dorsal and posterior end of cortical hem at E11.5 are distributed throughout nearly the entire cerebral cortical MZ along its dorsoventral axis by E14.5.

Tangential migratory behavior and localization of reelin-positive cells in the MZ of the cerebral cortex

To further characterize the spatial and temporal patterns of *in vivo* migratory behavior of CMWT-derived LacZ-positive descendants in the MZ, we monitored the sequential appearance of LacZ expression at the cerebral cortex in whole-mount preparation of the brain, after the electroporation of *LacZ* at E11.5 (Fig. 6). Focal restriction and reproducibility of electroporation-mediate gene transfer was confirmed beforehand (see supplemental Figs. 2–4, available at www.jneurosci.org). At E12.5, most of the cells that had incorporated *LacZ* remained at the CMWT where electroporation was conducted (Fig. 6*a*). Only a few, if any, cells traversed the edge of CMWT circumferentially from dorsal, ventral, and posterior directions, and emerged at the lateral wall of the cerebral hemisphere (Fig. 6*a*, inset). At E13.5, many LacZ-positive cells were located on the cortical surface along the entire dorsoventral axis of the posterior half of the cerebral cortex (Fig. 6*b*). By E16.5, the entire cortical surface was covered by intensive LacZ staining, especially at the posterior cerebral cortex (Fig. 6*c*). The LacZ staining was also detected on the ventral cortical surface (Fig. 6*c*, inset), which was consistent with the observations of the migratory behavior of the LacZ descendants on E12.5 sections (Fig. 5*h,I*) (see also Fig. 4*b*, inset). There was a caudomedial-high to rostrolateral-low gradient in the distribution of LacZ-positive cell populations, as it was observed at E14.5 (Fig. 4*b,d*). The extent of anterior limit of LacZ-positive cells on the cortical surface

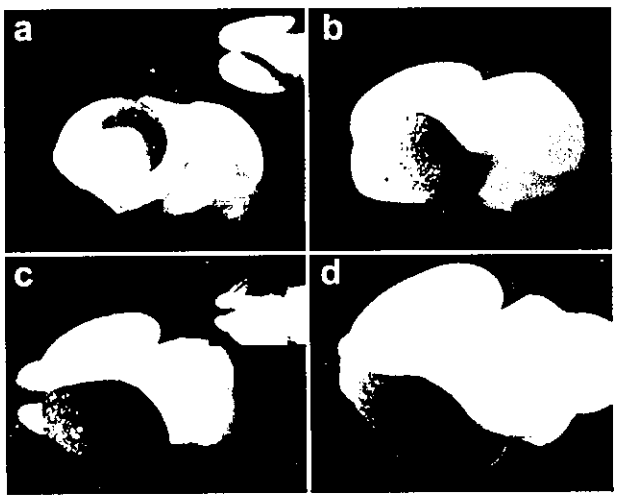

Figure 6. *In vivo* tangential migratory behavior of the CMWT-derived LacZ descendants. Whole-mount images showing the tangential migratory behavior of LacZ descendants on the cortical surface of E12.5 (*a*) ($n = 8$: electroporated samples), E13.5 (*b*) ($n = 4$), E16.5 (*c*) ($n = 5$), and E18.5 (*d*) ($n = 2$) brains. Inset in *a*, A dorsal view. Inset in *c*, A ventral view.

remained essentially similar from E14.5 onward, suggesting that CMWT-derived reelin-positive cells at E11.5 may have reached at their final destination at around E14.5 (Figs. 4*b,d*, 6*c*). From E16.5 onward, LacZ-positive cells harbored extensive tangentially oriented neurites, a characteristic morphology of many of the matured reelin-positive cells (Fig. 6*c*). At E18.5, intensive LacZ staining covered the entire cerebral cortex in a gradient apparently similar to that observed from E14.5 onward (Fig. 6*d*).

Together, these results obtained from the *in vivo* studies provide evidence that a substantial population of prospective reelin-positive cells is generated at the CMWT, including the cortical hem at E11.5, and tangentially migrate to the MZ of the cerebral cortex. They traverse the edge of the CMWT circumferentially and appear at the lateral wall of the cerebral hemisphere to set up an overall posterior–anterior stream of cells. Subsequently, they are widely distributed throughout the entire neocortex in a caudomedial-high to rostrolateral-low gradient and, consequently, comprise a substantial population of reelin-positive cells located at the posterior neocortex.

In vitro slice culture analyses of origins and migratory behavior of reelin-positive cells

The *in vivo* analyses presented above, however, is retrospective in nature and do not rule out the possibility that LacZ-positive cells located in the neocortical MZ originated from locations where no LacZ staining remained after the *in vivo* culture period.

To rule out this possibility and to further examine the tangential migratory pathways taken by the CMWT-derived reelin-positive cells, we set up an *in vitro* slice culture experiment that allowed us to analyze the origins and migratory behavior of reelin-positive cells prospectively on time during the culture period (Fig. 7). We electroporated *GFP* into the CMWT of ICR mice at E11.5 and permitted embryos to develop *in vivo* until 24 hr after the electroporation, when the level of gene expression is expected to be reached nearly at the peak. We isolated embryos and selected for the telencephalon in which GFP expression was detected only at the CMWT. Then, slices were prepared from the selected telencephalon (Fig. 7*l*), cultured *in vitro*, and were monitored on time for the migratory behavior of GFP-positive cells using GFP fluorescent. We prepared slices along the dorsolateral, pos-

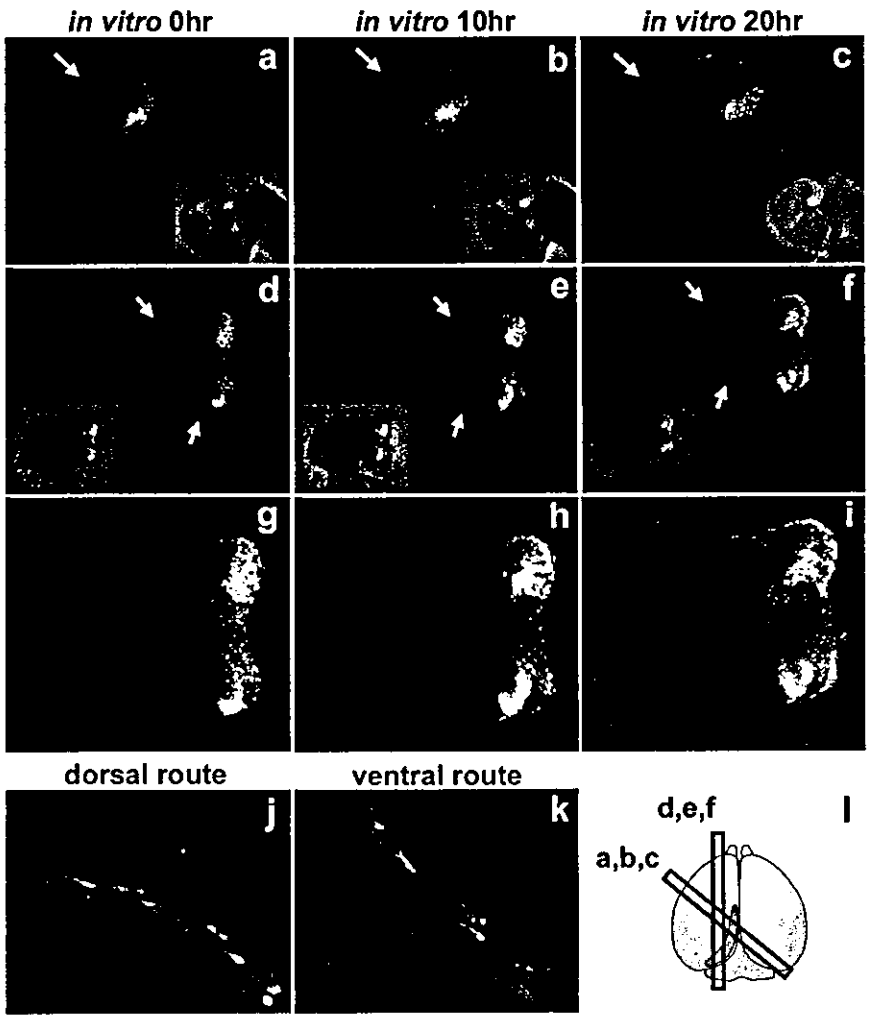

Figure 7. *In vitro* slice culture analyses on the origins and migratory pathway of CMWT-derived descendants. *a–i*, Images obtained after 0 hr (*a, d, g*), 10 hr (*b, e, h*), and 20 hr (*c, f, i*) of *in vitro* slice cultures prepared from caudomedial–rostrolateral sections (*a–c*) and posterior–anterior sections (*d–i*). Insets (*a–f*) show the merged images of fluorescent and bright field. *g–i*, High-power views of *d–f*. *j, k*, Tangentially migrating GFP-positive descendants on dorsal (*g*), and ventral (*h*) routes. *l*, A diagram showing the way slices were prepared through the electroporated regions at the CMWT. Arrows (*a–f*) show the extent of tangential migration. Images are representative of 19 slices obtained from eight electroporated samples.

terior–anterior, or caudomedial–rostrolateral axis of the cerebral cortex through the CMWT where the electroporation-mediated gene transfer was conducted, and asked which slices were preferred by the CMWT-derived GFP-positive descendants to tangentially migrate in the MZ *in vitro*.

In slice cultures prepared from the sections along the dorsolateral axis, GFP-positive descendants did not migrate along the cortical surface over the 24 hr of the culture period (data not shown). In contrast, in slice cultures from sections along either the caudomedial–rostrolateral or posterior–anterior axis, many tangentially migrating descendants from the CMWT were detected along the cortical surface of the prospective neocortex over the 20 hr of the culture period (Fig. 7*a–i*). At the time of isolation only a few GFP-expressing descendants were detected at the prospective neocortex (Fig. 7*a,d,g*). The number of descendants increased markedly after 10 hr (Fig. 7*b,e,h*), and the population extended from medial to lateral along the cortical surface over 20 hr of culture period (Fig. 7*c,f,i*). Dorsal and ventral migratory routes in an overall posterior–anterior direction were recognizable, which was consistent with the results obtained from the *in vivo* studies (Fig. 7*a–i*). Forwardly extended tangentially oriented neurites tailed by the following cell bodies, a characteristic feature of migrating cells, were detected in both dorsal (Fig. 7*j*) and ventral (Fig. 7*k*) route of migration.

Thus, these *in vitro* slice culture experiments provide prospective and direct evidence that progenitor cells located at the CMWT at E11.5 generate descendants that tangentially migrate on the neocortical surface. Moreover, these studies suggest that the CMWT-derived descendants take an overall posterior–anterior directed pathway on the neocortical surface along the caudomedial–rostrolateral axis and posterior–anterior axis, but not preferentially along the dorsolateral axis of the cerebral cortex.

Discussion

Present studies address three major points on the issues dealing with the ontogeny of reelin-positive MZ cells: (1) The CMWT, including the cortical hem, appears to be a source for the generation of prospective reelin-positive cells. (2) The CMWT-derived reelin-positive cells tangentially migrate at the cortical MZ in an overall posterior–anterior direction. (3) These migrating neurons distribute in a caudomedial-high to rostrolateral-low cellular gradient throughout the entire neocortex during the peak period of corticogenesis.

Our results define neocortical reelin-positive marginal zone cells, in addition to neocortical interneurons (Anderson et al., 1997), as a neuronal subtype that tangentially migrates from locations extrinsic to the neocortex and participates in the neocortical organization. Unlike the migration of interneurons, it appears there is a strict preference in the migration of CMWT-derived reelin-positive cells in that these neurons migrate exclusively in the MZ. Furthermore, our findings define a population of neocortical reelin-positive cells as a subclass of reelin-positive cells derived commonly from the CMWT and distributed throughout the entire cerebral cortical MZ.

Differential reelin-positive cell marker expression and the heterogeneity of reelin-positive cells

We first consider the relationship between the GFP expression and reelin-positive cells in *Tg* mouse embryos. Previous studies on the analyses of early expression patterns of reelin-positive cell markers raised the possibility that reelin-positive cells are generated from several putative sources in the telencephalon (Schiffmann et al., 1997; Alcantara et al., 1998). Our results presented above indicate that *GFP* transgene, in addition to reelin and p73, serves as another reliable marker for the identification of reelin-positive cells that are located in *Tg* embryonic neocortical MZ. The spatial and temporal correlations between the expressions of *GFP* with those of *reelin* and *p73* from the early onset of reelin-positive cell development suggest that *GFP* expression and reelin-